Extracting Reynolds Stresses from Acoustic Doppler Current Profiler Measurements in Wave-Dominated Environments

JOHANNA H. ROSMAN, JAMES L. HENCH, JEFFREY R. KOSEFF, AND STEPHEN G. MONISMITH

Environmental Fluid Mechanics Laboratory, Stanford University, Stanford, California

(Manuscript received 22 August 2006, in final form 1 May 2007)

ABSTRACT

Surface waves introduce velocity correlations that bias and often dominate Reynolds stress estimates made using the traditional variance method for acoustic Doppler current profilers (ADCPs). This analysis shows that the wave bias is the sum of a real wave stress and an error due to instrument tilt, both of which have a large uncertainty. Three alternative extensions to the variance method for calculating Reynolds stress profiles from ADCP measurements in wavy conditions are analyzed. The previously proposed variance fitting method (Variance Fit) is evaluated and two more general methods that use along- and between-beam velocity differencing with adaptive filtering (Vertical AF and Horizontal AF) are derived. The three methods are tested on datasets containing long-period monochromatic swell (Moorea, French Polynesia) and shorter-period mixed swell (Santa Barbara, California). The Variance Fit method leaves a residual wave bias in beam velocity variances, especially for intermediate waves, but gives physically reasonable Reynolds stress estimates because most of the residual wave bias cancels when the variance method is applied. The new Vertical AF method does not produce inherent wave bias in beam velocity variances, but yields comparable Reynolds stresses to the Variance Fit method. The Horizontal AF method performs poorly for all but monochromatic waves. Error remaining after one of the above methods is applied can be attributed to residual wave error, correlation of turbulence between points chosen for differencing, or correlation between waves and turbulence. A simple procedure is provided for determining the minimum bin separation that can be used.

1. Introduction

Turbulent stresses, or Reynolds stresses, represent the transport of momentum by turbulence and thus can control the vertical structure of turbulent environmental flows. Knowledge of Reynolds stresses along with mean velocity profiles allows the eddy viscosity, the most common parameterization of vertical mixing due to turbulence, to be computed. In the shallow coastal ocean, measurement of Reynolds stresses is complicated by the presence of surface waves. Although for small-amplitude irrotational waves the horizontal and vertical components of wave orbital velocities are 90° out of phase and therefore should have zero covariance, very small tilts in sensor alignment, or real wave stress associated with a sloping bed, for example, lead to a covariance between horizontal and vertical velocities that can contaminate or even dominate Reynolds stress measurements. Additionally, waves often occupy the same frequency range as turbulence in the shallow coastal ocean, and therefore wave contamination cannot be removed by simple frequency filtering.

Historically, two classes of methods have been used to remove wave bias from Reynolds stress measurements. Pressure–velocity correlation methods remove components of the velocity signal that are correlated with pressure or surface elevation (e.g., Benilov and Filyushkin 1970; Agrawal and Aubrey 1992); however, these methods fail to adequately remove wave bias when there is directional spread in the wave field (Herbers and Guza 1993). Velocity differencing methods (Trowbridge 1998; Shaw and Trowbridge 2001; Feddersen and Williams 2007) use the property that the spatial scale over which wave orbital velocities are coherent is much larger than the scale over which turbulent velocity fluctuations are coherent. Direct velocity differencing between measurements that are separated in space

Corresponding author address: Johanna H. Rosman, Environmental Fluid Mechanics Laboratory, Civil and Environmental Engineering, Stanford University, Stanford, CA 94305-4020.
E-mail: jrosman@stanford.edu

DOI: 10.1175/2007JTECHO525.1

has been used successfully to remove the wave component of horizontal velocity variations for sensors that are closely spaced compared with the wavelength of a wave (Trowbridge 1998). The range of applicability of this method has been extended by allowing the velocities at the two locations to be related by a linear transform before differencing (Shaw and Trowbridge 2001; Feddersen and Williams 2007).

These methods allow Reynolds stress to be measured in wavy conditions at a limited number of points; however, the ultimate goal is to measure full profiles of turbulent quantities. Lohrmann et al. (1990) introduced a method for calculating Reynolds stress profiles from four-beam current profiler measurements using the difference between the velocity variances along opposing beams. Stacey et al. (1999a), Lu and Lueck (1999), and Williams and Simpson (2004) extended this work with analyses of the confidence in Reynolds stress measurements. The variance method has since been applied successfully in a number of studies of stratified tidal systems (Stacey et al. 1999b; Rippeth et al. 2002; Fugate and Chant 2005). Comparisons with independent collocated acoustic Doppler velocimeter (ADV) measurements have validated the method (Souza and Howarth 2005; Nidzieko et al. 2006) and illustrated that the fast pinging rate mode 12 maintains accuracy while reducing noise relative to the single ping mode 1 (Nidzieko et al. 2006; Williams and Simpson 2004). However, application of the variance method to coastal seas has illustrated that the method fails in the presence of energetic surface waves (Rippeth et al. 2003; Howarth and Souza 2005; Souza and Howarth 2005).

Uncertainty in the principal axes of wave orbital motion leads to a wave bias in Reynolds stresses calculated using the variance method, similar to that described above for point velocity measurements. Velocity differencing methods are a viable option for removing wave contamination from Reynolds stress profiles calculated using the variance method. Whipple et al. (2006, hereafter WLS) proposed a method to remove wave contamination by differencing along-beam velocities measured at different bins of the same acoustic Doppler current profiler (ADCP) beam, based on the method introduced by Trowbridge (1998). The decay of wave velocity between bins chosen for differencing is determined from a fit to the vertical profile of the variance of beam velocity. The variance fitting method assumes that wave orbital velocities decay with depth in accordance with linear wave theory, that velocities decay in the same way with depth for opposite beams, and that velocities at different points along the ADCP beam are perfectly in phase, a condition that is seldom satisfied.

In this paper, we analyze the limitations of the WLS Variance Fit method and develop two more general methods for extracting Reynolds stresses from wave-contaminated ADCP data. These new methods, based on Shaw and Trowbridge (2001), make no assumption about the form of the decay of wave orbital velocities with depth, and they allow for a phase lag between measurements used for differencing. We evaluate and cross-compare the three methods using field measurements containing long-period monochromatic swell (Moorea, French Polynesia) and short-period mixed swell (Santa Barbara, California). The remainder of this paper is organized as follows: section 2 describes the field sites, deployment details, and hydrodynamic conditions during the experiments; section 3 sets up the problem and derives expressions for the bias introduced by waves; section 4 details the Variance Fit method and presents the two new approaches to removing the wave bias; the three methods are cross-compared and the limitations of each method are discussed in section 5, and key findings are summarized in section 6.

2. Overview of field deployments

This paper draws on data from two experiments, one in Moorea, in December 2005, and the other in Santa Barbara, in March 2005. For each experiment, a 1.2-MHz four-beam broadband ADCP (RD Instruments Workhorse monitor) was deployed on the bottom, looking upward, in approximately 10 m of water. The instrument was programmed to operate in fast pinging mode 12, recording one velocity profile per second. Each recorded velocity was the average of six measurements (subpings) at a 40-ms separation. Velocities were recorded in beam coordinates; that is, one along-beam velocity was obtained for each of the instrument's four acoustic beams. Local wave statistics and thermal stratification were measured in both experiments (Sea-Bird SBE26, SBE26+, SBE39). The following two sections give background information about the two field sites, details relating to the individual deployments, and a summary of hydrodynamic conditions during the experiments.

a. Moorea deployment: 8–18 December 2005

The Moorea experiment was conducted approximately 1.2 km offshore of the north shore of Moorea (17°28.8′S, 149°50.4′W; Fig. 1a). This part of the Moorea shoreline is characterized by a shallow back-reef area (0–1 km from shore), a sharp reef crest where wave breaking occurs, and a forereef area (1–1.5 km) from shore. Beyond the forereef, the seafloor drops off

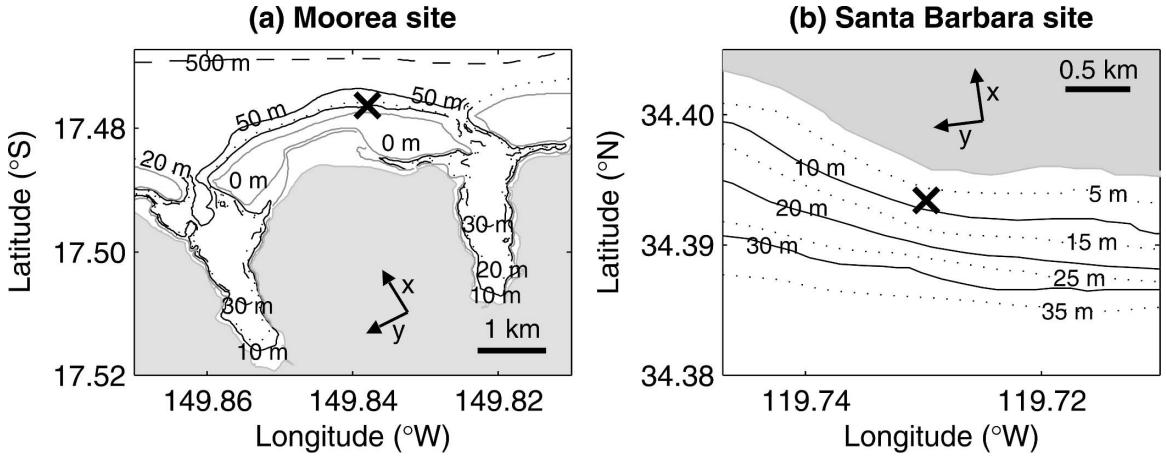

FIG. 1. Maps of the two field sites, (a) Moorea and (b) Santa Barbara, showing the coastline (land area shaded gray), depth contours relative to MSL, and instrument locations, marked with an X. Instrument orientation is indicated by the *x*–*y* axes, with the *x* axis directed from beam 2 to beam 1 and the *y* axis directed from beam 4 to beam 3.

quickly, reaching a 500-m depth at about 2 km from shore. Thus, the site is fully exposed to long-period ocean swell, which is commonly generated in the North Pacific during the austral summer (Bromirski et al. 2005). The forereef is characterized by raised reef areas inhabited by fine corals and deeper sand channels running perpendicular to the shore. The instruments were deployed near the head (shoreward end) of one of these sand channels in water 11.7 m deep, although the adjacent reef area was as shallow as 6–8 m. The tidal range is very small (about 0.2 m) at this site.

The ADCP bin size was 0.25 m, with the first bin 1.0 m above bottom. The ADCP was deployed to be as level as possible, but the instrument tilt varied between 0° and 3° during the experiment because of scour around the frame. The instrument heading (angle clockwise from north to beam 3, *y* axis) was 240°. The thermistor string contained 10 loggers (Sea-Bird, SBE39), recording temperature every 5 s, positioned at 1-m intervals from 0.5 to 9.5 m above bottom. Temperature data are not available for the first 2.5 days of the experiment because of a delay in the thermistor string deployment.

Observed conditions during the experiment are summarized in Fig. 2. Currents near the bed remained low (less than 0.05 m s^{-1}) throughout, presumably because the instrument was located in a deeper sand channel, with raised reef areas immediately alongshore in both directions. Velocities near the surface reached 0.2 m s^{-1}, and the majority of velocity shear occurred between 4 and 8 m above bottom. During the first part of the experiment, gradient Richardson numbers indicate that the water column was well mixed, without sufficient vertical stratification to suppress shear generation of turbulence. During the latter part of the experiment, stratification increased and was usually sufficient to inhibit vertical mixing. Significant wave periods ranged from 12 to 20 s, and significant wave heights reached as high as 1.5 m. The beginning of the experiment saw the tail end of a swell event from offshore, a further two swell events occurred during the experiment period, and the last four days saw much less wave activity. The dominant wave direction was from the north (heading 345°–360°), at an angle of 60°–75° from the ADCP *y* axis.

b. *Santa Barbara deployment: 23 March–8 April 2005*

The second field site was offshore of Mohawk Reef (34°23.7′N, 119°43.8′W), west of the town of Santa Barbara in Southern California (Fig. 1b). The instruments were deployed in an area with a sandy bottom, about 40 m offshore of a rocky reef that is seasonally covered with a dense kelp forest. The average water depth at the measurement location was 9.3 m and the tidal range was 2 m.

The ADCP bin size was 0.5 m and the first bin was 1.3 m from the bottom. The ADCP pitch and roll remained less than 2.5° throughout the experiment, and the instrument heading was 261°. A thermistor string was collocated with the ADCP, with SBE39 temperature loggers at 1-m intervals between 1 and 7 m above bottom recording at 30-s intervals.

The hydrodynamic conditions during the Santa Barbara deployment are shown in Fig. 2. Current direction was predominantly alongshore and reversed on a mixed semidiurnal/diurnal basis. Current speeds regularly exceeded 0.3 m s^{-1}, and the majority of the velocity shear

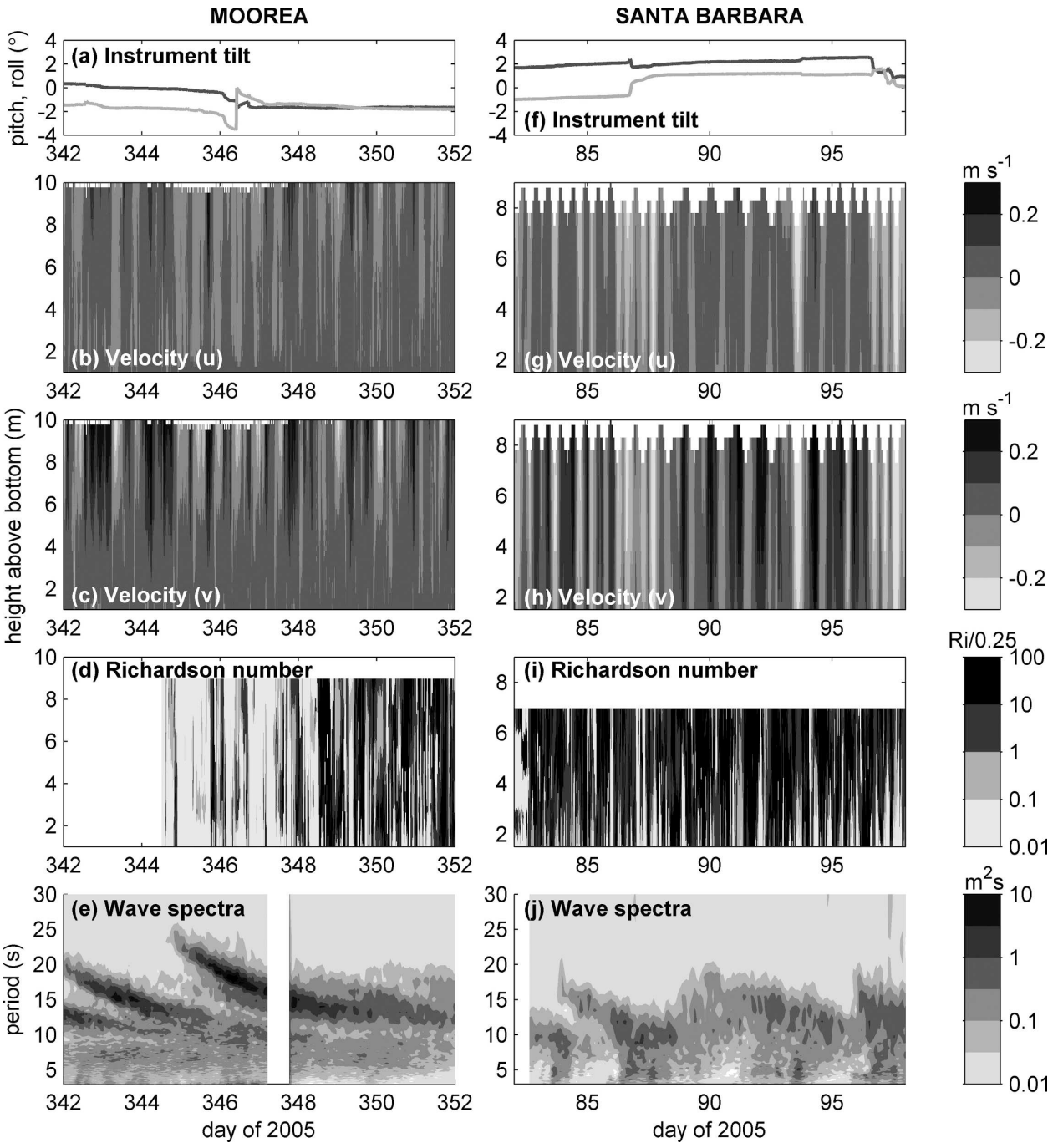

FIG. 2. Conditions during the experiments: (a), (f) instrument tilt (pitch and roll); (b), (g) 10-min-averaged currents in the *x* direction; (c), (h) 10-min-averaged currents in the *y* direction; (d), (i) Richardson numbers calculated from interpolated velocity and temperature profiles; and (e), (j) wave amplitude spectral density as a function of wave period and time. The data gap in (e) is due to instrument servicing.

was near the seabed. Gradient Richardson numbers, calculated from 10-min-averaged velocity and temperature profiles, exceeded 0.25 30% of the time in the lower water column and 55% of the time in the upper water column, indicating that stratification was often sufficient to suppress vertical turbulent mixing. Significant wave periods ranged from 5 to 15 s, and significant wave heights varied between 0.5 and 1.3 m. Wave spectra were broad, with both a wide swell peak (7–15 s), and a wind wave peak (4–5 s). The dominant wave

direction was from the southwest (220°–240°), at an angle of 20°–40° from the ADCP y axis.

3. The variance method and wave bias

a. Coordinate systems

A four-beam ADCP typically has two pairs of opposing transducers that emit acoustic pulses along "beams," as depicted in Fig. 3. Along-beam velocities are calculated by the instrument firmware, from the Doppler shift in the sound signal returned to the transducers, yielding four along-beam velocities (u_1, u_2, u_3, u_4), defined to be positive toward the instrument. Beam velocities can be resolved into an orthogonal coordinate system that is fixed relative to the ADCP. We use the coordinate system defined by Lu and Lueck (1999), where $x^\dagger$ is the direction from beam 2 to beam 1, and $y^\dagger$ is the direction from beam 4 to beam 3 (Fig. 3). Beam velocities (u_1, u_2, u_3, u_4), expressed in terms of velocities in the instrument coordinate system ($u^\dagger$, $v^\dagger$, $w^\dagger$), are

$$\begin{aligned} u_1 &= -u^\dagger \sin\theta - w^\dagger \cos\theta \\ u_2 &= u^\dagger \sin\theta - w^\dagger \cos\theta \\ u_3 &= -v^\dagger \sin\theta - w^\dagger \cos\theta \\ u_4 &= v^\dagger \sin\theta - w^\dagger \cos\theta, \end{aligned} \tag{1}$$

where θ is the half angle between opposing beams (20° for an RDI Workhorse ADCP). In the case of a perfectly level instrument, $u^\dagger$ and $v^\dagger$ correspond to horizontal velocities and $w^\dagger$ corresponds to the vertical velocity.

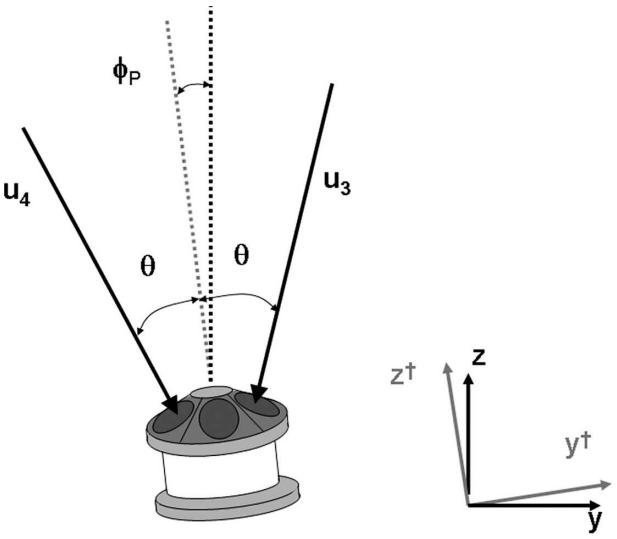

FIG. 3. The ADCP beam geometry and coordinate systems: the ($y^\dagger$, $z^\dagger$) coordinate system relative to the instrument and the (y, z) coordinate system relative to earth. The pitch angle is denoted ϕ_P.

If an ADCP is tilted by a pitch angle ϕ_P about the x axis (positive counterclockwise) or by a roll angle ϕ_R about the y axis (positive counterclockwise), the transform from the instrument coordinate system ($u^\dagger$, $v^\dagger$, $w^\dagger$) to a level coordinate system (u, v, w) is

$$\begin{bmatrix} u \\ v \\ w \end{bmatrix} = \begin{bmatrix} \cos\phi_R & 0 & \sin\phi_R \\ \sin\phi_P \sin\phi_R & \cos\phi_P & -\sin\phi_P \cos\phi_R \\ -\cos\phi_P \sin\phi_R & \sin\phi_P & \cos\phi_P \cos\phi_R \end{bmatrix} \begin{bmatrix} u^\dagger \\ v^\dagger \\ w^\dagger \end{bmatrix}. \tag{2}$$

For small ϕ_P and ϕ_R, this expression can be simplified using Taylor expansions. Retaining only terms to first order in ϕ_P and ϕ_R yields

$$\begin{bmatrix} u \\ v \\ w \end{bmatrix} = \begin{bmatrix} 1 & 0 & \phi_R \\ 0 & 1 & -\phi_P \\ -\phi_R & \phi_P & 1 \end{bmatrix} \begin{bmatrix} u^\dagger \\ v^\dagger \\ w^\dagger \end{bmatrix}. \tag{3}$$

Inverting this equation gives an expression for ($u^\dagger$, $v^\dagger$, $w^\dagger$) in terms of the coordinates (u, v, w):

$$\begin{bmatrix} u^\dagger \\ v^\dagger \\ w^\dagger \end{bmatrix} = \begin{bmatrix} 1 & 0 & -\phi_R \\ 0 & 1 & \phi_P \\ \phi_R & -\phi_P & 1 \end{bmatrix} \begin{bmatrix} u \\ v \\ w \end{bmatrix}. \tag{4}$$

b. Introduction to the variance method

In the absence of waves, each component of the velocity can be decomposed into a mean (e.g., $\bar{v}$) associated with slowly varying flow and into a fluctuation (e.g., v') associated with turbulence. Mean values are calculated over an appropriate time interval (e.g., 10 min) for which the flow is statistically stationary. If each quantity in Eq. (1) is decomposed in this way, it can be shown (Lohrmann et al. 1990; Stacey et al. 1999a) that

$$\begin{aligned} -\overline{u^{\dagger\prime} w^{\dagger\prime}} &= \frac{\overline{u_2'^2} - \overline{u_1'^2}}{4 \sin\theta \cos\theta} \\ -\overline{v^{\dagger\prime} w^{\dagger\prime}} &= \frac{\overline{u_4'^2} - \overline{u_3'^2}}{4 \sin\theta \cos\theta}. \end{aligned} \tag{5}$$

This is the variance method for calculating Reynolds stresses from ADCP beam velocities.

Substituting the transformation in Eq. (4) into Eq. (5) yields

$$\frac{\overline{u_2'^2} - \overline{u_1'^2}}{4\sin\theta\cos\theta} = -\overline{u'w'} - \phi_R(\overline{u'^2} - \overline{w'^2}) + \phi_P\overline{u'v'}$$

$$\frac{\overline{u_4'^2} - \overline{u_3'^2}}{4\sin\theta\cos\theta} = -\overline{v'w'} + \underbrace{\phi_P(\overline{v'^2} - \overline{w'^2}) - \phi_R\overline{u'v'}}_{E_{\text{turb}}}, \tag{6}$$

in agreement with Lu and Lueck (1999). Here, E_{turb} is the bias introduced to Reynolds stress estimates by instrument tilt in the absence of waves. For the worst case of highly anisotropic turbulence, $\overline{u'^2} - \overline{w'^2} \sim \overline{u'v'} \sim 5\overline{u'w'}$ (e.g., Lu and Lueck 1999; Gross and Nowell 1983), yielding a maximum bias of 50% for a tilt of 3° (0.05 rad). However, in general, bias terms will be smaller, and for isotropic turbulence $\overline{u'^2} - \overline{w'^2} \to 0$ and $\overline{u'v'} \sim \overline{u'w'}$, yielding a bias of about 5% for a tilt of 3°.

c. Bias introduced by waves

In the presence of waves, the situation is somewhat more complicated. We derive the equations and present results for the y direction in this section; however, the analysis for the x direction is identical and the results are similar. The instantaneous velocity can be decomposed into a mean (e.g., $\overline{v}$) associated with the slowly varying flow, a component associated with the waves (e.g., $\tilde{v}$), and a fluctuation associated with the turbulence (e.g., v'). For example,

$$\begin{aligned} v &= \overline{v} + \tilde{v} + v' \\ w &= \overline{w} + \tilde{w} + w'. \end{aligned} \tag{7}$$

Since the wave and turbulence components cannot be separated by simple frequency filtering, direct application of the variance method gives

$$\begin{aligned} \frac{\overline{(\tilde{u}_4 + u_4')^2} - \overline{(\tilde{u}_3 + u_3')^2}}{4\sin\theta\cos\theta} &= -\overline{(\tilde{v}^\dagger + v^{\dagger\prime})(\tilde{w}^\dagger + w^{\dagger\prime})} \\ &= -\overline{\tilde{v}^\dagger\tilde{w}^\dagger} - \overline{v^{\dagger\prime}w^{\dagger\prime}}. \end{aligned} \tag{8}$$

The simplification in the second line of Eq. (8) assumes that the wave and turbulence components of the signal are uncorrelated. Equation (8) can then be transformed to a level coordinate system using Eq. (4):

$$\begin{aligned} &\frac{\overline{(\tilde{u}_4 + u_4')^2} - \overline{(\tilde{u}_3 + u_3')^2}}{4\sin\theta\cos\theta} \\ &\quad = -\overline{v'w'} \underbrace{-\overline{\tilde{v}\tilde{w}}}_{E_{\text{ws}}} + \underbrace{\phi_P(\overline{\tilde{v}^2} - \overline{\tilde{w}^2}) - \phi_R\overline{\tilde{u}\tilde{v}}}_{E_{\text{tilt}}} \\ &\qquad + \underbrace{\phi_P(\overline{v'^2} - \overline{w'^2}) - \phi_R\overline{u'v'}}_{E_{\text{turb}}}. \end{aligned} \tag{9}$$

As in the no-waves case, the turbulence contribution to the error, E_{turb}, is less than 50% for tilts less than 3°; however, as we show below, the wave terms in Eq. (9) can dominate the Reynolds stress estimates as the wave orbital velocities can be orders of magnitude larger than turbulent fluctuations. The errors due to wave bias can be categorized as 1) E_{ws}, the real wave stress ($-\overline{\tilde{v}\tilde{w}}$), or 2) E_{tilt}, the error due to the interaction of wave orbital velocities and instrument tilt [$\phi_P(\overline{\tilde{v}^2} - \overline{\tilde{w}^2}) - \phi_R\overline{\tilde{u}\tilde{v}}$]. For an instrument with one pair of beams aligned with the direction of wave motion, $\phi_R\overline{\tilde{u}\tilde{v}} \to 0$. Note also that for deep water waves with near-circular particle orbits, $\overline{\tilde{v}^2} \approx \overline{\tilde{w}^2}$ and thus $\phi_P(\overline{\tilde{v}^2} - \overline{\tilde{w}^2}) \to 0$.

A tilt in the principal axes of wave orbital motion from the horizontal, associated with a sloping bed, for example, can lead to a large E_{ws}. If v_{w} and w_{w} are the wave velocities in a coordinate system rotated to the principal axis of wave orbital motion, α is the angle between the y axis and the direction of wave propagation, and ξ is the angle between the principal axis of wave orbital motion and the horizontal, then the resulting wave stress is

$$\begin{aligned} E_{\text{ws}} &= -\overline{\tilde{v}\tilde{w}} \\ &= -\overline{(v_{\text{w}}\cos\xi\cos\alpha - w_{\text{w}}\sin\xi)(v_{\text{w}}\sin\xi\cos\alpha + w_{\text{w}}\cos\xi)} \\ &= -(\overline{v_{\text{w}}^2}\cos^2\alpha - \overline{w_{\text{w}}^2})\sin\xi\cos\xi - \overline{v_{\text{w}}w_{\text{w}}}\cos2\xi\cos\alpha \\ &\approx -(\overline{v_{\text{w}}^2}\cos^2\alpha - \overline{w_{\text{w}}^2})\sin\xi\cos\xi, \end{aligned} \tag{10}$$

which is nonzero even if the correlation between components of wave orbital velocity in the rotated coordinate system ($\overline{v_{\text{w}}w_{\text{w}}}$) is zero.

The effect of wave bias can be seen in the uncorrected Reynolds stresses, obtained by applying the variance method [Eq. (5)] directly to the Moorea and Santa Barbara measurements (Fig. 4). The wave biases due to instrument tilt (E_{tilt}) and wave orbital orientation (E_{ws}) were calculated using Eqs. (9) and (10), respectively. In this calculation, it was assumed that wave velocities did not vary significantly between opposite beams, and thus the beam velocities could be combined in a sensible way, using Eqs. (1) and (2), to calculate the instantaneous horizontal and vertical components of wave orbital velocities. Additionally, turbulent velocity fluctuations were assumed to be small compared to wave velocities, and total de-meaned velocities were therefore used in Eqs. (9) and (10).

The uncertainties in the ADCP pitch and roll cause an uncertainty in the calculated E_{tilt} and E_{ws}. The accuracy and precision of the tilt sensor are each 0.5° (RD Instruments 2005). Because $N = 600$ individual pitch and roll measurements were averaged to obtain the 10-

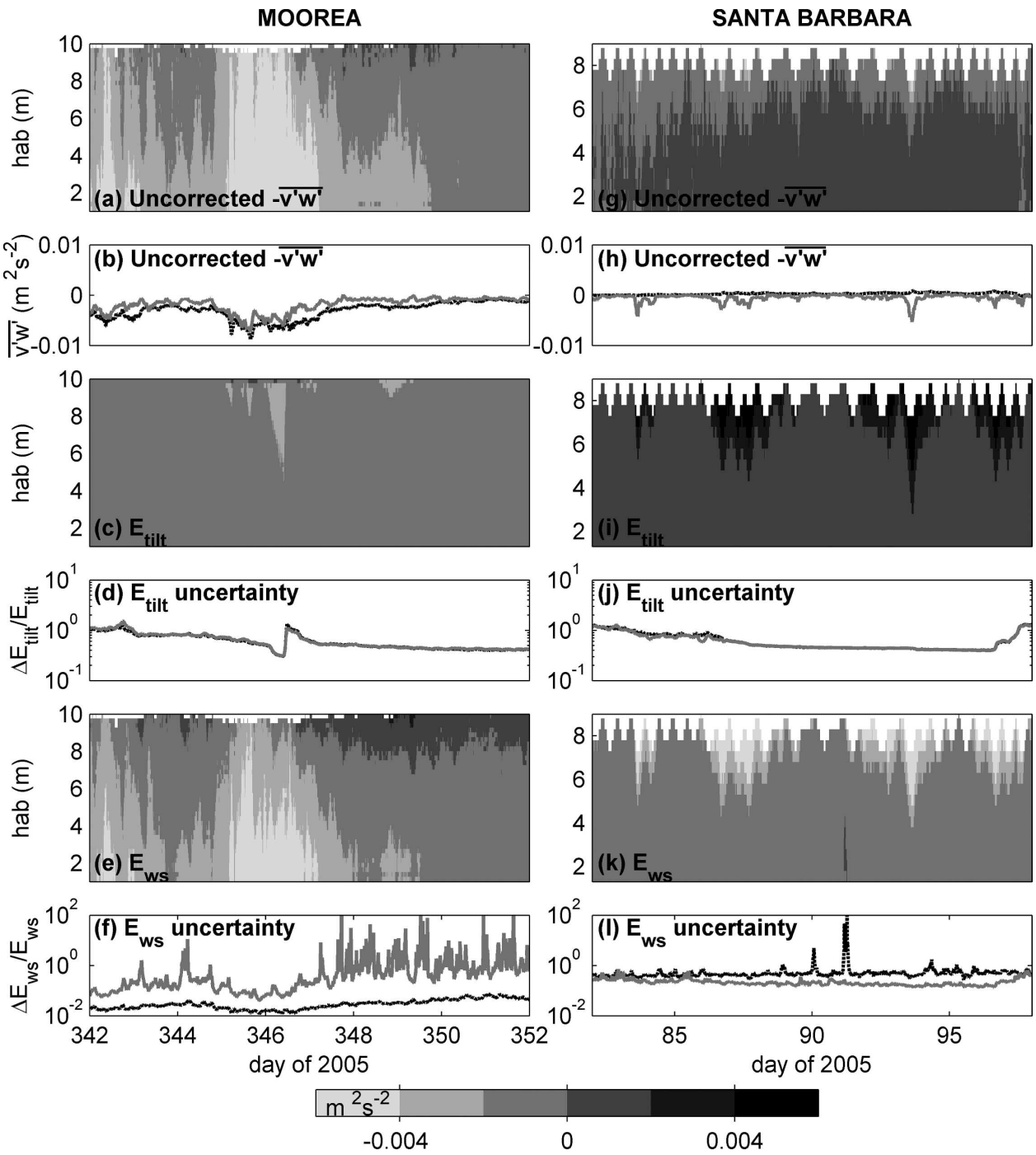

FIG. 4. Effect of wave contamination on computed Reynolds stress values: (a), (g) uncorrected Reynolds stress profiles calculated directly using the variance method; (b), (h) uncorrected Reynolds stresses (1.3 mab, black) near bottom and (8 mab for Moorea, 6.8 mab for Santa Barbara, gray) near surface; (c, i) contoured error due to instrument tilt [E_{tilt}, Eq. (10)]; (d), (j) fractional uncertainty in E_{tilt} (black) near bottom and (gray) near surface; (e), (k) contoured error due to variation of the principal axis of wave orbitals from horizontal [E_{ws}, Eq. (9)]; and (f), (l) fractional uncertainty in E_{ws} (black) near bottom and (gray) near surface.

min averages, and the precisions of ϕ_P and ϕ_R in Eq. (9) and ξ in Eq. (10) are $0.5°/\sqrt{N} = 0.0204°$. As the accuracy is not reduced by averaging, the total uncertainties (accuracy plus precision) in the 10-min-averaged ϕ_P, ϕ_R, and ξ are 0.53°. The uncertainties in E_{tilt} and E_{ws} as a result of the tilt uncertainty were computed using standard propagation of error procedures. Fractional uncertainties in E_{ws} are small for the Moorea dataset

but large for the Santa Barbara dataset, and fractional uncertainties in E_{tilt} are large in both experiments (Fig. 4).

The main source of wave bias in the Moorea Reynolds stress estimates is E_{ws}, which is larger near the bottom where wave motion was aligned with the steeply sloping seafloor. The fractional uncertainties in the estimates of E_{ws} for Moorea are relatively small because the angle between the horizontal and the wave principal axis (8°–25°) is much larger than the accuracy of the tilt sensor (0.5°). In the Santa Barbara Reynolds stress estimates, E_{ws} and E_{tilt} are similar in magnitude but opposite in direction and largest near the surface where wave orbital velocities were greatest. However, the fractional uncertainties in these terms are large because the tilt sensor accuracy is large compared with the instrument tilt and compared with the angle between the horizontal and the wave orbital motion. The sum of E_{ws} and E_{tilt} explains 99% of the variance of the uncorrected Reynolds stress near the bottom for the Moorea data and 97% of the observed variance near the surface. For the Santa Barbara data, the wave bias terms explain 95% of the variance of uncorrected Reynolds stress near the bottom and 80% near the surface.

Above, we estimated the uncertainty in E_{tilt} and E_{ws} based on the uncertainty in instrument tilt alone. Nonlinear waves can result in a nonzero correlation between wave velocity components even if velocities are rotated to the principal axes of wave orbital motion (i.e., $\overline{v_w w_w} \neq 0$). Also, we are unable to determine wave velocities accurately because opposing beams are separated in space. These factors further increase the uncertainty in estimates of E_{tilt} and E_{ws} computed from Eqs. (9) and (10). As it is not possible to determine E_{tilt} and E_{ws} accurately enough to isolate the true Reynolds stresses, we seek alternative methods for removing wave contamination from the beam velocities prior to applying the variance method.

4. Wave bias correction methods

In this section we present three methods for removing wave bias from beam velocities and subsequent Reynolds stress estimates: the Variance Fit method of WLS, a vertical differencing method incorporating adaptive filtering (Vertical AF), and a horizontal (between beam) differencing method incorporating adaptive filtering (Horizontal AF).

a. Variance Fit method

The Variance Fit method, based on Trowbridge (1998) and extended to ADCPs by WLS, assumes that wave orbital velocities are in phase along any one ADCP beam and decay with depth according to linear wave theory. The analysis presented in this section illustrates that the first of these assumptions is usually poor, even for the case of low-frequency linear waves, because the along-beam velocity contains components of both horizontal and vertical wave orbital velocities, which are 90° out of phase and decay with depth below surface in a different way.

Transforming the theoretical expressions for $\tilde{u}$ and $\tilde{w}$ from linear wave theory (e.g., Dean and Dalrymple 1991) into beam coordinates yields the following expression for the beam velocity variance, for a beam axis aligned with the direction of wave propagation:

$$\overline{\tilde{u}_{\text{beam}}^2} = c_1[\cosh c_2(z + h) - \cos 2\theta], \tag{11}$$

where

$$c_1 = \frac{H^2\omega^2}{16 \sinh^2 kh},$$

$$c_2 = 2k$$

$\tilde{u}_{\text{beam}}$ is the wave component of the beam velocity, θ is the half angle between opposing beams, H is wave height, ω is wave frequency, k is wavenumber, h is the total water depth, and z is the vertical coordinate, defined to be zero at the surface and to be positive upward.

WLS assume that one of the ADCP beam pairs is oriented parallel to the direction of wave propagation. However, it can be shown that for a beam pair oriented at some angle α to the direction of wave propagation, the expression for beam velocity variance as a function of depth is

$$\overline{\tilde{u}_{\text{beam}}^2} = c_1[(\cos^2\alpha \sin^2\theta + \cos^2\theta) \cosh c_2(z + h) + (\cos^2\alpha \sin^2\theta - \cos^2\theta)], \tag{12}$$

where c_1 and c_2 are defined as in Eq. (11).

The beam velocity time series are segmented into intervals over which the flow is statistically stationary (Δt, here 10 min), and the means are removed from the beam velocities over these time intervals. Henceforth, u_{beam} refers to the de-meaned beam velocity. The direction of wave propagation relative to the instrument (α) is computed from the principal axes of wave orbital motion for each interval. Here $\overline{u_{\text{beam}}^2}$ is calculated over each interval, and the expression in Eq. (12) is fit to each variance profile to obtain the parameters c_1 and c_2. To remove the wave component of the beam velocity, two bins are selected at levels $z^{(1)}$ and $z^{(2)}$, centered on the height at which the Reynolds stress is required and spaced far enough apart that the turbulence is not cor-

related. The appropriate choice of bin separation is discussed in section 5c. The beam velocities at the two heights are differenced according to

$$\Delta u_{\text{beam}} = u^{(1)}_{\text{beam}} - \beta u^{(2)}_{\text{beam}}, \tag{13}$$

where

$$\beta = \sqrt{\frac{\overline{(\tilde{u}^{(1)}_{\text{beam,fit}})^2}}{\overline{(\tilde{u}^{(2)}_{\text{beam,fit}})^2}}} \tag{14}$$

is computed from the variance fit [Eq. (12)]. Then,

$$\begin{aligned} \Delta u_{\text{beam}} &= u'^{(1)}_{\text{beam}} - \beta u'^{(2)}_{\text{beam}} + \Delta\tilde{u}_{\text{beam}} \\ \overline{\Delta u_{\text{beam}}{}^2} &= \overline{u'^{(1)}_{\text{beam}}{}^2} + \beta^2\overline{u'^{(2)}_{\text{beam}}{}^2} + \epsilon_{\text{wave}} + \epsilon_{\text{turb}} + \epsilon_{\text{wt}}, \end{aligned} \tag{15}$$

where

$$\begin{aligned} \epsilon_{\text{turb}} &= -2\beta\overline{u'^{(1)}_{\text{beam}} u'^{(2)}_{\text{beam}}} \\ \epsilon_{\text{wave}} &= \overline{\Delta\tilde{u}_{\text{beam}}{}^2} \\ \epsilon_{\text{wt}} &= 2\overline{(u'^{(1)}_{\text{beam}} - \beta u'^{(2)}_{\text{beam}})\Delta\tilde{u}_{\text{beam}}}. \end{aligned}$$

Here ϵ_{turb} is the error due to the correlation between the turbulence components at the two points chosen for differencing, which should reduce to zero for sufficient bin separation, ϵ_{wave} is the residual wave error, and ϵ_{wt} is the error that arises if there is a correlation between the velocity fluctuations due to waves and turbulence.

If the wave velocity decay factor β is the same for opposing beams, then application of the variance method [Eq. (5)] gives

$$\frac{\overline{\Delta u_4^2} - \overline{\Delta u_3^2}}{4\sin\theta\cos\theta} \approx -\overline{v'w'^{(1)}} - \beta^2\overline{v'w'^{(2)}}. \tag{16}$$

In WLS, β is chosen to be the average of the β values calculated for the two opposing beams. An estimate of the Reynolds stress in the y direction, between $z^{(1)}$ and $z^{(2)}$, is therefore

$$-\overline{v'w'^{(1-2)}} \approx \frac{\overline{\Delta u_4^2} - \overline{\Delta u_3^2}}{4\sin\theta\cos\theta(1+\beta^2)}. \tag{17}$$

The equation for $-\overline{u'w'}$ is analogous.

The Variance Fit method assumes that 1) the wave orbital velocities at the two chosen points are perfectly in phase, 2) the wave velocities decay with depth in accordance with linear wave theory, 3) the decay of the wave orbital velocities along opposite beams is the same ($\beta_3 = \beta_4 = \beta_{34}$), and 4) the waves are narrow spectrum and the wave period does not change substantially over the chosen averaging interval.

The first of these assumptions is usually poor and can lead to a large residual wave error in differenced beam velocity variances. The total phase difference between selected bins is the sum of two contributions. A small phase difference exists because of the time taken for a wave to propagate from the horizontal location of the first bin to the horizontal location of the second bin. For a vertical separation of 2 m, and a wave traveling parallel to a beam pair, there is a corresponding horizontal separation of $2\cos\theta$, which is 0.7 m for a 20° beam angle. The shallow- and deep-wave phase speeds are 9.9 and 6.2 m s^{-1}, respectively, in a 10-m water depth, leading to a maximum time delay between bins of 0.07–0.12 s for a wave traveling parallel to the beam.

There is also a phase difference due to the different relative amplitudes of the horizontal and vertical wave velocities at the selected bins. The amplitude of vertical velocity oscillations ($\tilde{w}$) decreases relative to the amplitude of horizontal velocity oscillations ($\tilde{v}$) with increasing depth below surface. Because $\tilde{w}$ and $\tilde{v}$ are 90° out of phase, this leads to a phase difference between along-beam velocities at different heights in the water column.

To assess the time delay and the size of the residual wave error in the corrected beam velocities due to this second type of phase difference, we applied the Variance Fit method to monochromatic waves with wave velocities computed from linear wave theory. Two waves are considered initially: a 4-s period, 0.3-m-high wave in 10 m of water, similar to the waves in the dataset used by WLS, and a 15-s period, 1-m-high wave in 10 m of water, similar to the waves seen in the present datasets. The variance fit [Eq. (12)] is computed from the wave parameters, and Eq. (13) is applied to a pair of points near the bed (1 and 3 m above bottom) and a pair of points near the surface (7 and 9 m above bottom). The resulting residual wave error in differenced beam velocity variance (Fig. 5) is small for the shorter 4-s waves. For the longer 15-s period waves, the residual wave error is reduced by two orders of magnitude by the Variance Fit method. However, the wave error in differenced beam velocity variances remains $O(10^{-4})$ m^2 s^{-2}, similar to the Reynolds stresses we are trying to measure.

The phase lag between bins and the resulting residual wave bias that can be expected in beam velocity variances after application of the Variance Fit method are shown in Fig. 6 as a function of kh and z. The residual wave error is small for short (deep water) waves because wave orbitals are close to circular, and the ratio of the amplitude of $\tilde{w}$ to the amplitude of $\tilde{v}$ varies little with vertical position, leading to relatively constant

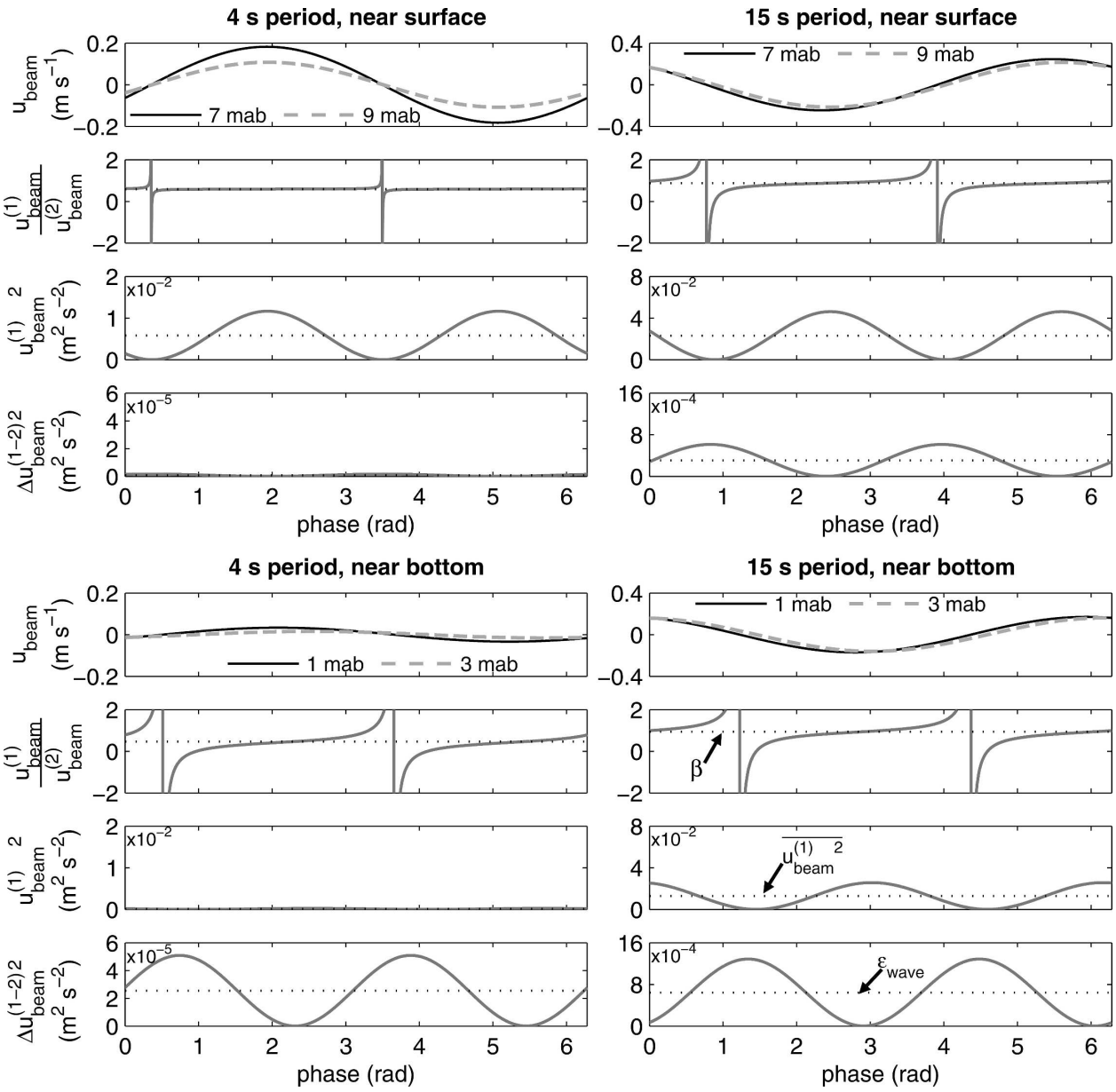

FIG. 5. Theoretical residual wave errors for Reynolds stresses calculated with the Variance Fit method for a monochromatic wave using linear wave theory. (left) A 4-s period, 0.15-m amplitude wave in 10 m of water; (right) a 15-s period, 0.5 m-amplitude wave in 10 m of water. (top) 8 m above bottom; (bottom) 2 m above bottom. Within each set of four time series, first: along-beam component of wave orbital velocity; second: ratio of velocity at the upper height to the velocity at the lower height, with (dotted) corresponding β from Eq. (13); third: square of the along-beam velocity prior to differencing, with (dotted) resulting wave bias; and fourth: remaining wave bias in along-beam velocity after correction, with (dotted) residual wave error.

phase in the along-beam component of wave orbital velocity with depth. The largest residual wave error occurs for intermediate waves with kh between 0.5 and 2 and is greatest in the lower part of the water column. For intermediate waves, the assumption of constant phase with depth is poor because $\tilde{w}$ decreases relative to $\tilde{v}$ with increasing depth below surface. For shallow-water waves, the assumption of constant phase is somewhat better than for intermediate waves because $\tilde{w}$ is always much smaller than $\tilde{v}$; thus the phase of the beam velocity signal is always dominated by the phase of the horizontal component of wave velocity.

b. *Vertical differencing with adaptive filtering*

Here we develop a new method using vertical differencing with adaptive filtering (Vertical AF) that is de-

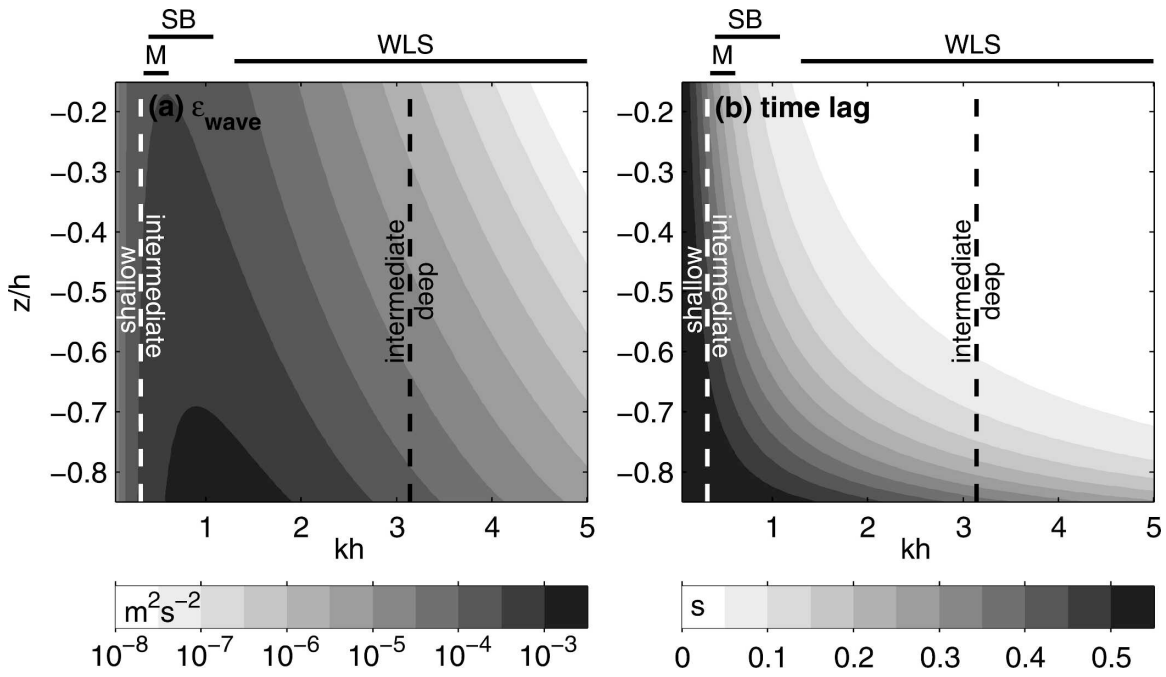

FIG. 6. Variation of (a) Variance Fit method residual wave error (ϵ_{wave}) and (b) time lag between beam velocities at $z^{(1)}$ and $z^{(2)}$ with wavelength and height above bottom for a monochromatic linear wave [where wave height is 1 m, water depth is 10 m, and separation between $z^{(1)}$ and $z^{(2)}$ is 2 m]. Wavenumber (k) and depth below surface (z) are normalized by the water depth (h). The range of wave conditions (kh) tested by WLS and those observed in the Moorea (M) and Santa Barbara (SB) deployments are indicated above the graphs.

signed to relax three assumptions associated with the Variance Fit method: 1) constant phase across the water depth, 2) decay with depth in accordance with linear wave theory, and 3) identical decay along opposite beams. The Vertical AF method is based on the method of Shaw and Trowbridge (2001), but it is extended here for use with ADCPs. Again we select two heights in the water column, $z^{(1)}$ and $z^{(2)}$, spaced a sufficient distance apart that turbulent velocity fluctuations are not coherent. Rather than assuming the wave velocity at $z^{(2)}$ is a constant multiplier of the wave velocity at $z^{(1)}$, we now assume that the wave velocity at $z^{(2)}$ is a linear function ($\mathcal{L}$) of the wave velocity at $z^{(1)}$. That is,

$$\tilde{u}^{(1)}_{\text{beam}}(t) = \mathcal{L}(\tilde{u}^{(2)}_{\text{beam}}) = \int_{-\infty}^{\infty} s(t^*)\tilde{u}^{(2)}_{\text{beam}}(t - t^*)\, dt^*, \quad (18)$$

where t is time, t^* is the integration variable, and $s(t)$ is a continuous function that relates $\tilde{u}^{(2)}_{\text{beam}}$ to $\tilde{u}^{(1)}_{\text{beam}}$.

In practice, we choose a time window size (L) and compute a linear function that best relates a velocity measurement at $z^{(1)}$ with a discrete sequence of velocity measurements of length L at $z^{(2)}$. That is, the predicted velocity $\hat{\tilde{u}}_{\text{beam}}$ at height $z^{(1)}$, based on measurements at $z^{(2)}$, is

$$\hat{\tilde{u}}^{(1)}_{\text{beam}}(t_i) = \sum_{j=-\frac{1}{2}(L-1)}^{\frac{1}{2}(L-1)} s_j u^{(2)}_{\text{beam}}(t_{i+j}), \quad (19)$$

where, again, u_{beam} implies the de-meaned beam velocity and $\mathbf{s}$ is now a vector of weights of length L that relate the discrete $\tilde{\mathbf{u}}^{(2)}_{\text{beam}}$ and $\tilde{\mathbf{u}}^{(1)}_{\text{beam}}$.

If $\mathbf{A}$ is a windowed matrix of the velocity data at point $z^{(2)}$, that is, the ith row of $\mathbf{A}$ is $[u^{(2)}_{\text{beam}}(t_{i-1/2(L-1)}), \ldots, u^{(2)}_{\text{beam}}(t_{i+1/2(L-1)})]$, Eq. (19) can be written in matrix form

$$\hat{\tilde{\mathbf{u}}}^{(1)}_{\text{beam}} = \mathbf{A}\mathbf{s}. \quad (20)$$

The vector of weights $\mathbf{s} = (s_1, \ldots, s_L)$ is chosen to minimize the sum of squared differences between predicted and measured beam velocities over each 10-min interval. We compute the weights following Shaw and Trowbridge (2001), whereby the estimator of the weights is

$$\hat{\mathbf{s}} = (\mathbf{A}^{\mathrm{T}}\mathbf{A})^{-1}\mathbf{A}^{\mathrm{T}}\mathbf{u}^{(1)}_{\text{beam}}. \quad (21)$$

The velocity difference at $z^{(1)}$ is then

$$\Delta u^{(1)}_{\text{beam}} = u^{(1)}_{\text{beam}} - \hat{\tilde{u}}^{(1)}_{\text{beam}}$$

$$= u'^{(1)}_{\text{beam}} - \mathcal{L}(u'^{(2)}_{\text{beam}}) + \Delta\tilde{u}^{(1)}_{\text{beam}}, \quad (22)$$

and the beam velocity variances are computed as

$$\overline{\Delta u^{(1)}_{\text{beam}} u^{(1)}_{\text{beam}}} = \overline{[u'^{(1)}_{\text{beam}} - \mathcal{L}(u'^{(2)}_{\text{beam}}) + \Delta\tilde{u}^{(1)}_{\text{beam}}][u'^{(1)}_{\text{beam}} + \tilde{u}^{(1)}_{\text{beam}}]} = \overline{u'^{(1)\,2}_{\text{beam}}} + \epsilon_{\text{wave}} + \epsilon_{\text{turb}} + \epsilon_{\text{wt}}, \tag{23}$$

where

$$\epsilon_{\text{wave}} = \overline{\tilde{u}^{(1)}_{\text{beam}} \Delta\tilde{u}^{(1)}_{\text{beam}}}$$
$$\epsilon_{\text{turb}} = -\overline{\mathcal{L}(u'^{(2)}_{\text{beam}})(u'^{(1)}_{\text{beam}})}$$
$$\epsilon_{\text{wt}} = 2\overline{\tilde{u}^{(1)}_{\text{beam}} u'^{(1)}_{\text{beam}}} - \overline{\mathcal{L}(u'^{(2)}_{\text{beam}})\tilde{u}^{(1)}_{\text{beam}}} - \overline{\mathcal{L}(\tilde{u}^{(2)}_{\text{beam}}) u'^{(1)}_{\text{beam}}}.$$

Here, ϵ_{wave} is the residual wave error, ϵ_{turb} is the error due to correlation between turbulence at $z^{(1)}$ and the linear transform of the turbulence component at $z^{(2)}$, and ϵ_{wt} is the wave–turbulence correlation error. Since the Vertical AF method allows a phase difference between the chosen points, we expect that the residual wave error will be much smaller than that of the Variance Fit method. If the bins for differencing are separated sufficiently, then ϵ_{turb} will be zero. The wave–turbulence correlation error ϵ_{wt} is the sum of an error due to the correlation between waves and turbulence at $z^{(1)}$, and an apparent correlation will appear between waves and turbulence due to the method used to compute the linear transform $\mathcal{L}$.

The Reynolds stresses can then be computed by applying the variance method; for example, for the y direction,

$$\frac{\overline{\Delta u^{(1)}_4 u^{(1)}_4} - \overline{\Delta u^{(1)}_3 u^{(1)}_3}}{4\sin\theta\cos\theta} \approx -\overline{v'w'^{(1)}}. \tag{24}$$

The expression for the x direction is analogous.

Note that the Vertical AF method is set up here as the product of a differenced quantity and an undifferenced quantity. It can be shown (see the appendix) that for the Vertical AF method the variance computed from the differenced along-beam velocity multiplied by the undifferenced along-beam velocity $[\Delta u^{(1)}_{\text{beam}} u^{(1)}_{\text{beam}}]$ is exactly equivalent to the variance computed from the square of the differenced along-beam velocity $[\Delta u^{(1)\,2}_{\text{beam}}]$ because of properties of the linear transform $\mathcal{L}$. That is, the errors associated with the two computation methods are mathematically identical.

Although the Vertical AF method theoretically allows for a phase shift between beam velocities at the heights selected for differencing, typical phase shifts in the range of 0.1 to 0.5 s can cause substantial residual wave error (Fig. 6). Because our measurement frequency is 1 Hz (the maximum ping rate for mode 12), we are unable to fully resolve such phase shifts, leaving potential for residual wave bias in Reynolds stress estimates. The use of a sequence of measurements (rather than a single measurement as in the Variance Fit method) for computing the linear transfer function is expected to improve the phase resolution beyond the sample interval of 1 s.

c. Horizontal differencing with adaptive filtering

Here we derive a second method (Horizontal AF) incorporating adaptive filtering, which involves horizontal (between beam) differencing rather than vertical (within beam) differencing. For a standard 20° ADCP beam angle, the horizontal distance between opposite beams at any vertical location is 0.73 multiplied by the height above the instrument. Since the largest turbulence length scales at any height in the water column are typically equal to or less than the height above bottom, we assume that the requirement that turbulent velocities are not correlated between points is automatically satisfied. The Horizontal AF method increases the range of heights at which Reynolds stresses can be calculated because it does not require a pair of points that are separated in the vertical. Additionally, it has the potential to decrease the wave bias error further because both points used for differencing are at the same depth below surface, and thus the highest frequency detectable waves will be the same for both points.

The velocity at some height z along beam a is predicted from the measurement at the same height z along the opposite beam b. Here, $\mathbf{A}$ becomes a windowed matrix of the beam b velocity at height z, and the predicted beam a velocity is given by

$$\hat{\tilde{\mathbf{u}}}_a = \mathbf{A}_b \mathbf{s}. \tag{25}$$

The weights $\mathbf{s}$ are computed using Eq. (21). The velocity difference at z is

$$\Delta u_a = u_a - \hat{\tilde{u}}_a, \tag{26}$$

and the variance method is applied as in Eq. (24) to calculate the Reynolds stresses.

5. Discussion and method evaluation

a. Cross-comparison of results from the three methods

The three methods described in section 4 were applied to bin pairs throughout the water column for both

the Moorea and Santa Barbara measurements. A vertical bin separation of 2 m was used for the Variance Fit and Vertical AF methods (see section 5c for details on bin separation). For the Vertical AF method, window lengths (L) of 9 and 7 s were used for the Moorea and Santa Barbara measurements, respectively, close to half of the dominant wave period during times of higher wave energy. For the Horizontal AF method, a window length close to one full wave period was used (17 s for Moorea, 13 s for Santa Barbara). Choice of window lengths involved some trial and error, but were eventually chosen such that the peak of the transfer function **s** was well within the window length and weights reduced to zero at either end of the window. An averaging period of 10 min was used throughout. Results for the x and y directions were qualitatively similar. We present only the results for the y (beams 3 and 4) direction here, which most closely aligned with the dominant current direction and thus was the direction with a larger Reynolds stress signal.

To evaluate each method, beam velocity power spectra were computed before and after correction. Spectra of beam 3 velocities throughout the water column are shown in Fig. 7 for a selected 6-h time period when both waves and currents were large. The uncorrected along-beam velocity spectra have wave peaks that are greatest near the surface, where wave orbital velocities are highest, and decay with depth. Note that the effects of wave energy at lower frequencies (e.g., the 20-s Moorea peak) are felt deeper into the water column than the effects of wave energy at higher frequencies (e.g., the 4-s Santa Barbara peak), as predicted by wave theory (e.g., Dean and Dalrymple 1991). It can be shown, in a similar way to the derivation of the variance method, that the cospectra of u and w can be computed as

$$P_{-uw} = \frac{P_{u4u4} - P_{u3u3}}{4 \sin\theta \cos\theta}, \tag{27}$$

where P_{u3u3} and P_{u4u4} are the power spectra of beam 3 velocity and beam 4 velocity, respectively, and θ is again the half angle between opposing beams. The magnitudes (absolute values) of the cospectra computed using Eq. (27) are shown in the bottom panels of Fig. 7.

The Variance Fit method removes the majority of the wave contamination in the beam velocities but leaves a residual wave bias at the dominant low-frequency wave peak for both datasets (0.05 Hz at Moorea, 0.08–0.1 Hz at Santa Barbara), as predicted in section 4a. Spectra for other beams and other time periods during the experiments indicate that the Variance Fit method consistently leaves a residual wave peak in beam velocity spectra. However, the residual wave peak is largely eliminated when the power spectra for opposite beams are differenced, and the wave peak is therefore not evident in the cospectra (Figs. 7f,l).

The Vertical AF method performs well at removing the wave peak from the beam 3 power spectrum over the chosen time period and produces a cospectrum that is very similar to the Variance Fit method. However, an examination of spectra for other time periods shows that the Vertical AF method also often leaves residual wave peaks. The presence of residual wave error is less consistent than for the Variance Fit method and depends on the quality of the linear function that can be obtained relating the beam velocity at $z^{(2)}$ to the beam velocity at $z^{(1)}$. This linear transformation may be poor if the phase difference between the two bins is not sufficiently resolved, if the wave period or direction changes significantly during the 10-min averaging period, or if wave orbital velocities are not the dominant component of velocity variations.

The Horizontal AF method performs poorly, consistently leaving a large residual wave peak in beam velocity power spectra and the cospectra obtained by differencing the power spectra for opposite beams. Theoretically, the Horizontal AF method should work well for linear, monochromatic waves because the velocity components along opposite beams have the same sinusoidal form, only shifted in phase. The problems encountered with this method in practice are attributed to the existence of asymmetric wave orbitals and the presence of a continuous spectrum of wave energy. Asymmetric wave orbitals may cause the wave orbital velocity to have a slightly different form along opposite beams, leading to poor coherence and the inability to adequately predict the wave velocity along one beam from the wave velocity along the opposite beam. Additionally, since beam velocities are related by a large phase shift, the Horizontal AF method may fail if the spectrum contains a superposition of waves of different frequencies and phases; that is, the wave form at time t may have a different form at time $t + \tau$, where τ is the phase shift for maximum correlation between the velocities along opposing beams.

Time series of Reynolds stress computed using each of the three methods are compared with uncorrected Reynolds stresses and depth-averaged currents in Fig. 8. For each field site, the results are shown for a region of high mean shear (6 m above bottom for Moorea, 2.3 m above bottom for Santa Barbara). The Horizontal AF method reduces the wave bias by a factor of about 5, but leaves a residual wave bias that continues to mask Reynolds stresses. Reynolds stresses computed using the Vertical AF and Variance Fit methods covary with mean currents and seem physically reasonable in both

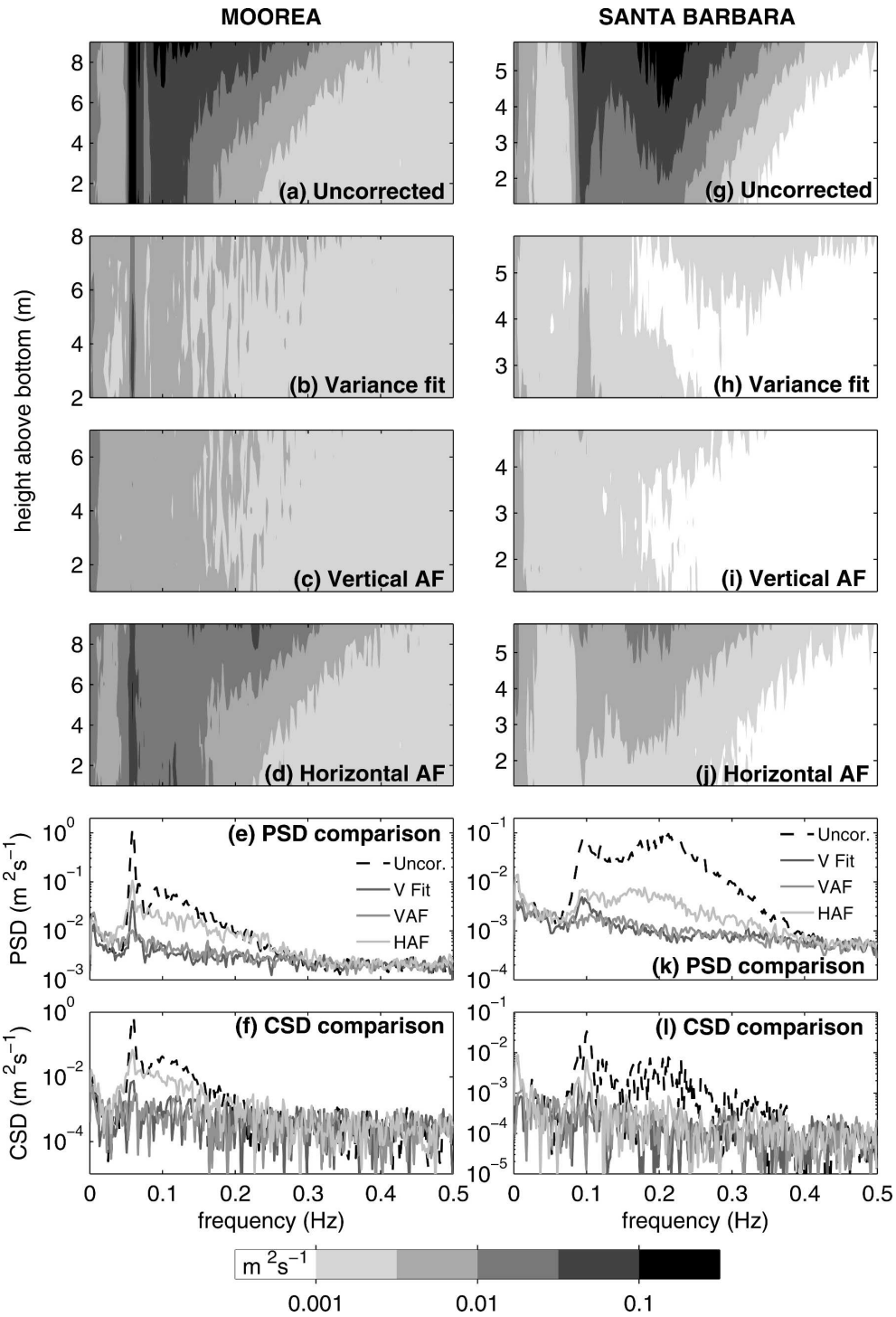

FIG. 7. The effects of velocity differencing methods on beam velocity power spectra: (a), (b), (c), (d), (g), (h), (i), (j) power spectra of (read across) beam 3 velocities and their variation with (read upward) height above bottom for a 3-h time period when wave amplitude was large; (e), (k) line graphs of power spectra at midwater column; (f), (l) line graphs of cospectra at midwater column computed from Eq. (27).

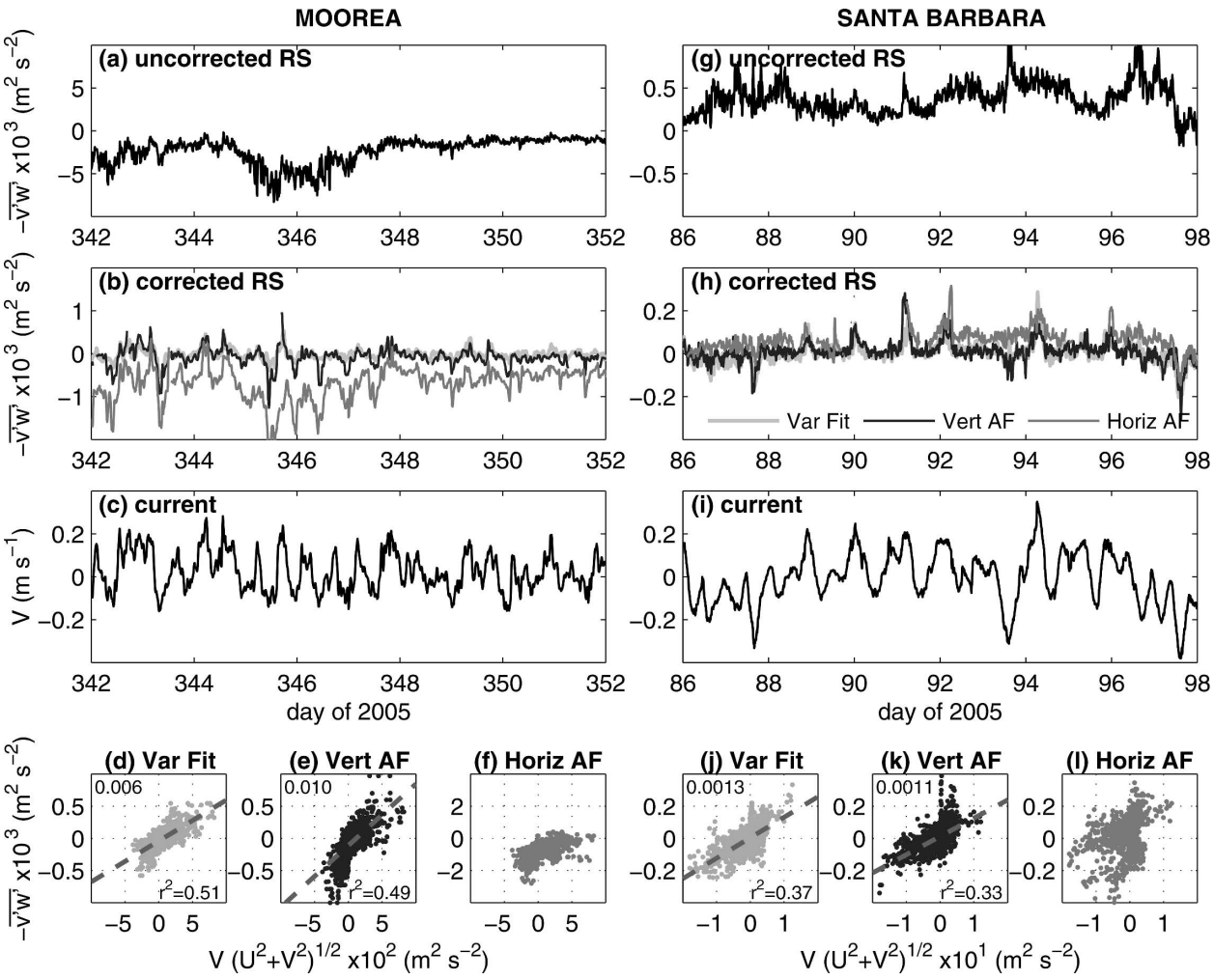

FIG. 8. Reynolds stresses calculated using the three velocity differencing methods: (a), (g) uncorrected Reynolds stress time series at a region of high shear in the water column (6 m above bottom for Moorea, 2.3 m above bottom for Santa Barbara); (b), (h) corrected Reynolds stresses; (c), (i) depth and time-averaged velocities; and (d), (e), (f), (j), (k), (l) scatterplots of Reynolds stresses versus 10-min-averaged velocities. Dashed lines are linear fits from which drag coefficients were deduced; slopes are indicated in the upper left, and *r*-squared values are in the lower right.

size and direction. Drag coefficients, calculated from the slope of the $-\overline{v'w'}$ versus $V\sqrt{U^2 + V^2}$ scatterplots, are 0.006–0.010 for Moorea, and 0.001–0.0012 for Santa Barbara. These values are consistent with drag coefficients reported in the literature for coral reefs (Reidenbach et al., 2006) and sandy beds (e.g., Dewey and Crawford 1988). The apparent success of the Variance Fit method is surprising given that it consistently leaves a residual wave bias in beam velocity variances (e.g., Fig. 7); however, the residual wave biases in opposing beam velocities are similar, and a large portion of the error cancels when the variance method [Eq. (17)] is applied.

Although both the Variance Fit and Vertical AF Reynolds stress estimates seem physically reasonable, they do not agree perfectly. Reynolds stresses computed using the Vertical AF method are 30% greater than those computed using the Variance Fit method for the upper-water column Moorea measurements, and 40% greater for the near-surface Santa Barbara measurements (Fig. 9). Near the bed, the Santa Barbara Vertical AF estimates are 25% smaller than the Variance Fit estimates, and the Moorea Vertical AF estimates are affected by a consistent negative bias. The following section explores the confidence we can have in Reynolds stresses estimated using the Variance Fit and Vertical AF methods.

b. Uncertainty in Reynolds stress estimates

Following the method of Stacey et al. (1999a), we derive estimates of the uncertainty in Reynolds stresses

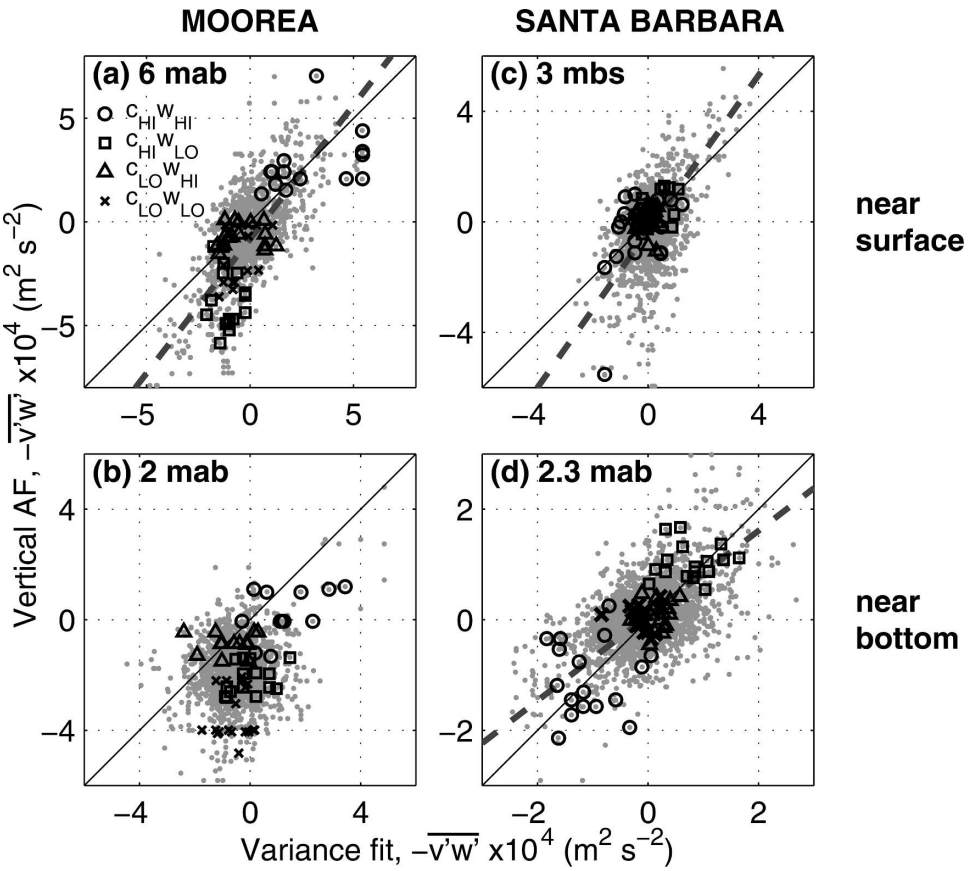

FIG. 9. Comparison of Reynolds stresses calculated using the Vertical AF and Variance Fit methods. The first row is near surface (3 m below surface) and the second row is near bottom (2 m above bottom). Open circles correspond to a chosen 3-h high-current, high-wave time period ($c_{HI}w_{HI}$), squares to a high-current, low-wave time period ($c_{HI}w_{LO}$), triangles to a low-current, high-wave time period ($c_{LO}w_{HI}$), and crosses to a low-current, low-wave time period ($c_{LO}w_{LO}$).

computed using the Vertical AF and Variance Fit methods. If we assume that consecutive Δu_{beam} values are independent and that Δu_3 and Δu_4 values are incoherent, then the variance of Reynolds stresses estimated using the Variance Fit method [Eq. (17)] is

$$\text{var}(\widehat{v'w'}) = \frac{\text{var}(\widehat{\Delta u_3^2}) + \text{var}(\widehat{\Delta u_4^2})}{16(1+\beta^2)\sin^2\theta\cos^2\theta}, \tag{28}$$

where $\widehat{v'w'}$ denotes the estimator of the Reynolds stress and $\widehat{\Delta u_{\text{beam}}{}^2} = (1/N)\Sigma_{i=1}^{N}\Delta u_{\text{beam}}(t_i)^2$ is the estimator of the variance of along-beam velocity fluctuations. As $\widehat{\Delta u_{\text{beam}}^2}$ is computed as the mean of N (here 600) individual $(\Delta u_{\text{beam}})^2$, we can employ the central limit theorem (e.g., Bendat and Piersol 2000) to give

$$\text{var}(\widehat{\Delta u_{\text{beam}}{}^2}) = \frac{1}{N}\text{var}(\Delta u_{\text{beam}}{}^2). \tag{29}$$

Using Eqs. (28) and (29), the variance of the Reynolds stress estimate can be computed directly from the individual $\Delta u_{\text{beam}}{}^2$ values.

Similarly, for the Vertical AF method, the variance of Reynolds stress estimates can be computed as

$$\text{var}(\widehat{v'w'}) = \frac{\text{var}(\widehat{u_3\Delta u_3}) + \text{var}(\widehat{u_4\Delta u_4})}{16\sin^2\theta\cos^2\theta} = \frac{1}{N}\frac{\text{var}(u_3\Delta u_3) + \text{var}(u_4\Delta u_4)}{16\sin^2\theta\cos^2\theta}. \tag{30}$$

The standard deviations of Reynolds stress estimates, computed using Eqs. (28)–(30), are shown in Fig. 10. In the top four panels of Fig. 10, the standard deviation of Reynolds stress is plotted against the Reynolds stress estimate, following Williams and Simpson (2004). The minimum measurement noise, given by the y intercept,

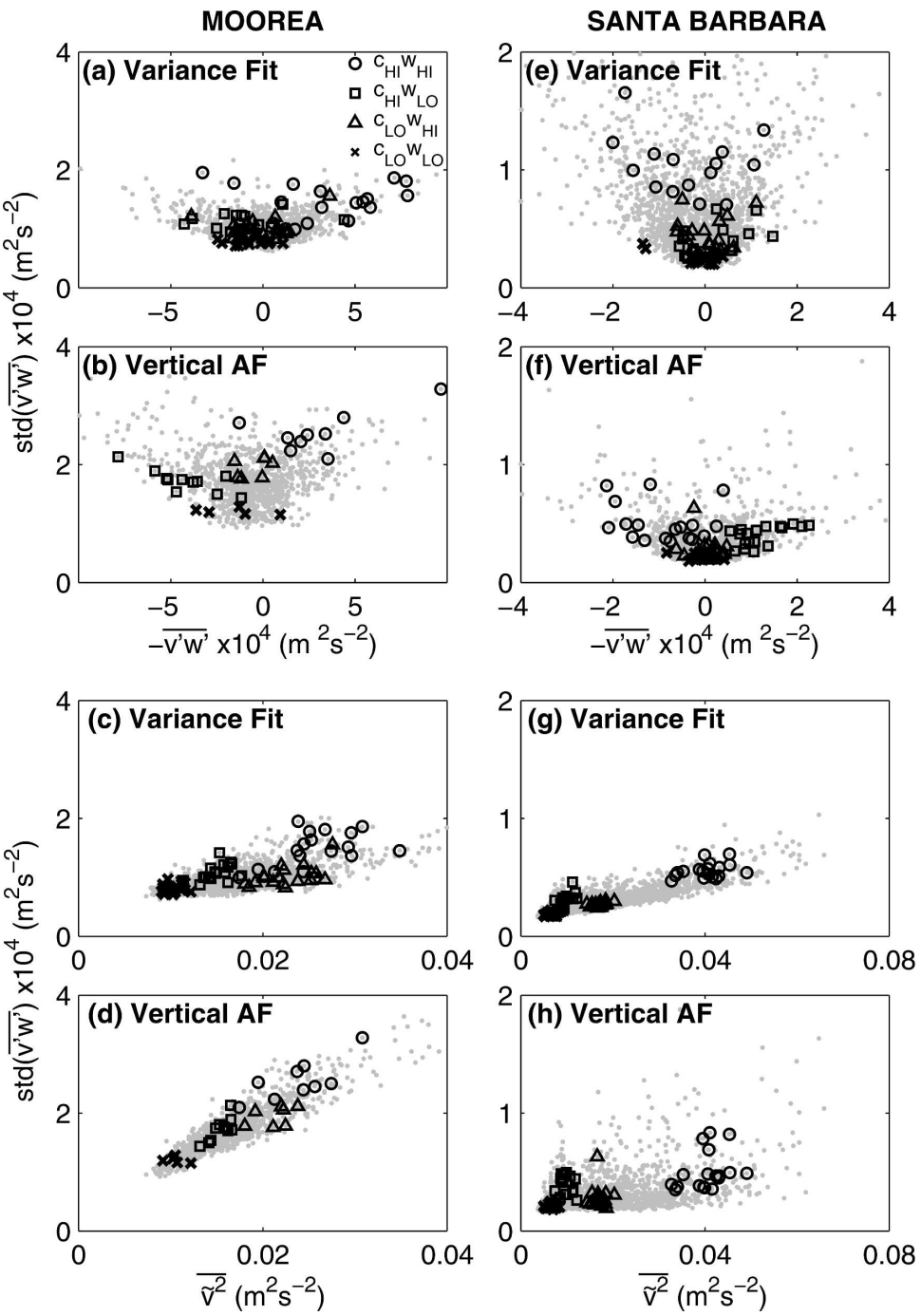

FIG. 10. Uncertainties in Reynolds stress estimates as a function of Reynolds stress for (a), (e) the Variance Fit method and (b), (f) the Vertical AF method, and as a function of wave orbital velocity for (c), (g) the Variance Fit method and (d), (h) the Vertical AF method. Results are for 6 m (M) and 2.3 m (SB) above bottom. Circles correspond to $c_{HI}w_{HI}$, squares to $c_{HI}w_{LO}$, triangles to $c_{LO}w_{HI}$, and crosses to $c_{LO}w_{LO}$.

is about 1×10^{-4} m^2 s^{-2} for the Moorea estimates, and 2×10^{-5} m^2 s^{-2} for the Santa Barbara estimates. Additionally, the Reynolds stress standard deviations for the low-wave time periods $c_{HI}w_{LO}$ and $c_{LO}w_{LO}$ are smaller than for the high-wave time periods $c_{HI}w_{HI}$ and $c_{LO}w_{HI}$ for the same Reynolds stress.

The variation of Reynolds stress standard deviations with wave orbital velocities are shown in the lower four

panels of Fig. 10. In all cases, the standard deviation of Reynolds stress increases monotonically with wave orbital velocity. If we assume that the relationship between Reynolds stress standard deviation and wave orbital velocity is linear and project the line of best fit back to zero wave velocity, then we obtain a minimum uncertainty of about 1.5×10^{-5} m^2 s^{-2}, similar to that obtained by Williams and Simpson (2004) and Nidzieko et al. (2006) for an ADCP operating in mode 12 in the absence of waves.

The uncertainty in Reynolds stress estimates, based on one standard deviation, for the Moorea measurements is about 1×10^{-4} m^2 s^{-2} when the waves are small and as large as 3×10^{-4} m^2 s^{-2} when the waves are large. For the Santa Barbara measurement, the uncertainty is 2×10^{-5} m^2 s^{-2} when waves are small and 1×10^{-4} m^2 s^{-2} when waves are large. These uncertainties are similar for both the Variance Fit and Vertical AF methods and indicate that when waves are large, uncertainties can be equal to or even greater than Reynolds stress estimates. Williams and Simpson (2004) show that the assumption of independence between consecutive beam velocities leads to underestimation of the variance of Reynolds stress estimates if consecutive measurements are correlated. Williams and Simpson multiply their variance estimates by a correction factor of γ_R determined from the autocorrelation function for u'^2_{beam}. From the autocorrelation function of $\Delta u_{\text{beam}}{}^2$ (Variance Fit) and $u_{\text{beam}}\Delta u_{\text{beam}}$ (Vertical AF) we estimate that γ_R varies between 1.8 and 4 for both methods. The Reynolds stress standard deviations are therefore a factor of 1.3–2 greater than those plotted in Fig. 10. To account for the nonindependence of consecutive measurements when estimating the uncertainties in Reynolds stresses computed for scientific applications, the variance can be corrected using the correction factor introduced by Williams and Simpson (2004).

c. *Sensitivity to bin separation for vertical differencing*

Both the Variance Fit method and the Vertical AF method rely on selecting two bins with sufficient vertical separation that the turbulent components of velocity are incoherent to eliminate ϵ_{turb}. However, wave components must be perfectly coherent between the two points (perfectly correlated for the Variance Fit method) to avoid a residual wave error ϵ_{wave}. Thus, the bin separation must be selected to provide a compromise between these competing issues. For the Variance Fit method, which does not allow for a phase difference between points chosen for differencing, the residual wave error is expected to increase with increasing bin separation, as the phase difference between velocities at the chosen bins increases. Additionally, for both methods, the residual wave error may increase with bin separation because shorter period waves are detectable closer to the surface.

To assess the behavior of the error terms (ϵ_{wave} and ϵ_{turb}) as a function of chosen bin separation, the beam variances (beams 3 and 4) and their difference from which Reynolds stress is derived were computed for a range of bin separations. The results are shown for a chosen height at which mean shear was large, for four time periods with different wave and current conditions in Fig. 11.

From Eqs. (15) and (23), the error due to turbulence correlation (ϵ_{turb}) acts to artificially decrease the variance of the along-beam velocity. The effect of turbulence correlation error is clearly seen in the Vertical AF results as the beam separation is increased from 0.5 to 1 to 2 m when currents are strong ($c_{\text{HI}}w_{\text{HI}}$ and $c_{\text{HI}}w_{\text{LO}}$) for both the Moorea and Santa Barbara datasets. This error term reduces to zero for bin separations greater than 2 m for the heights shown in Fig. 11. For each dataset and each z at which we computed Reynolds stresses, we constructed plots like those shown in Fig. 11 and deduced that 2 m was sufficient vertical separation. In general, the required bin separation will vary with position in the water column because of variation in the vertical length scales of turbulent structures. We therefore recommend that the analysis outlined above be done for each height at which Reynolds stresses are computed.

The residual wave error will always cause overestimation of the variance in along-beam velocities. For the Vertical AF method, there is little dependence of beam velocity variances on bin separation beyond the turbulence decorrelation scale; thus the Vertical AF method does not leave a consistent residual wave bias that is dependent on bin separation. However, for the Variance Fit method, the beam velocity variance increases consistently with increasing bin separation, and the calculated beam variance is strongly dependent on the chosen bin separation. This trend is likely due to the increasing phase separation between bins, and hence increasing residual wave error, with increasing bin pair separation. Note, however, that the difference between the velocity variances $\overline{u_3^2}$ and $\overline{u_4^2}$ does not vary much as bin separation increases, confirming that the Reynolds stress estimate is not significantly affected by this bias.

6. Summary and conclusions

This paper has provided an analysis of the error due to surface waves in Reynolds stresses computed using the variance method. Direct application of the variance

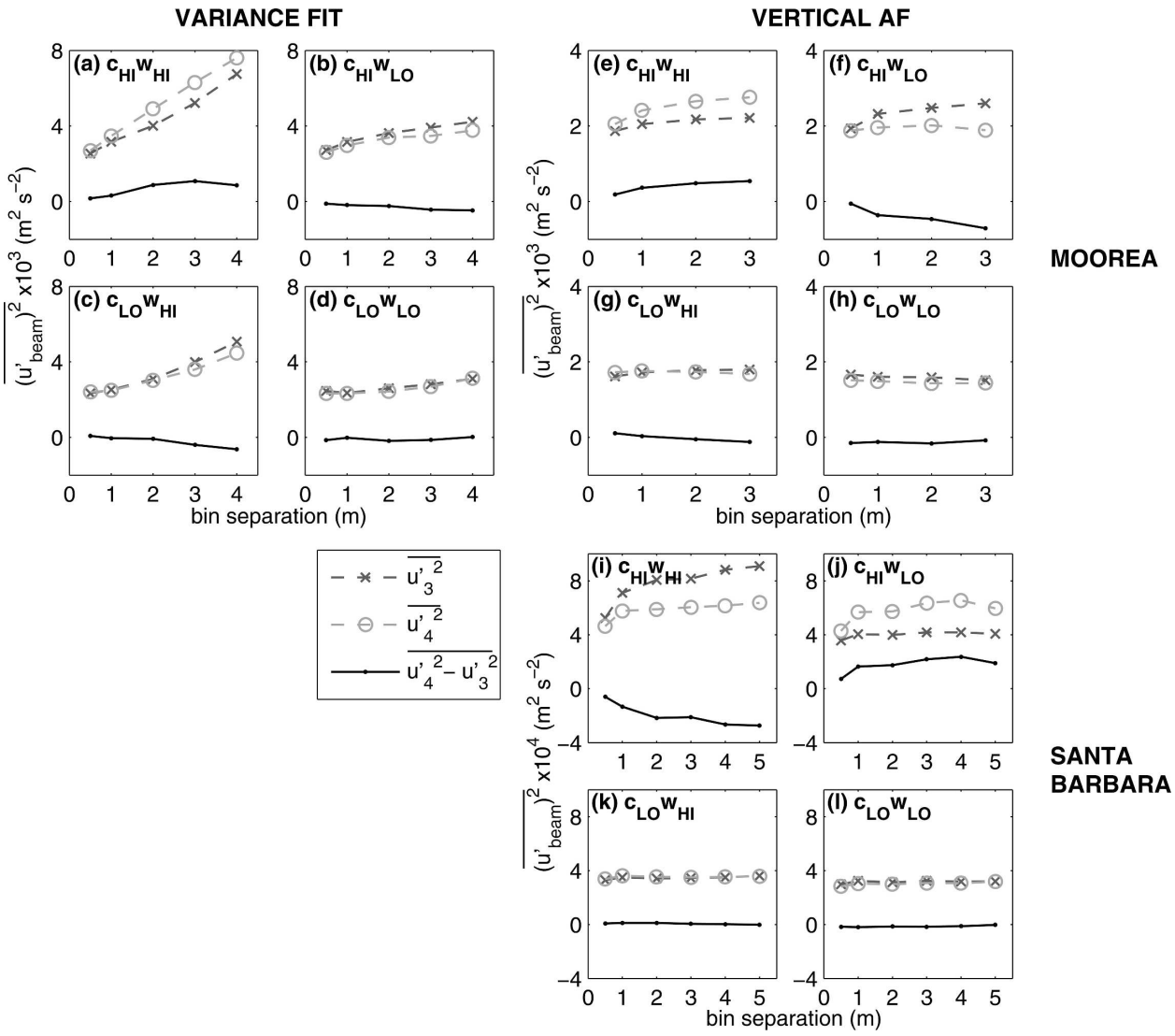

FIG. 11. Variation of Reynolds stress estimates with increasing bin separation. Panels within each set of four correspond to averages over the chosen 3-h periods $c_{HI}w_{HI}$, $c_{HI}w_{LO}$, $c_{LO}w_{HI}$, and $c_{LO}w_{LO}$.

method to wavy ADCP data results in a wave bias that, for the Moorea and Santa Barbara datasets, is an order of magnitude larger than the Reynolds stresses we are trying to measure. This wave bias is the sum of error due to instrument tilt and a real wave stress associated with the orientation of the principal axes of wave orbital motion. In some situations (e.g., the Moorea measurements) the real wave stress is the dominant bias term. The Reynolds stresses cannot be isolated by simply computing and subtracting the error terms, because the uncertainties in the error terms are too large.

Three methods for removing wave bias from beam velocities prior to application of the variance method have been derived and cross-compared. Vertical differencing with variance fitting (Variance Fit), proposed by WLS, was shown to perform well for short waves near the surface, where the phase difference between beam velocities at vertically separated points is small. For longer waves, a significant residual wave bias remains in the beam velocities after differencing; however, reasonable Reynolds stress estimates are obtained because most of the residual wave error is canceled when the variance method is applied. Vertical differencing with adaptive filtering (Vertical AF) generally performs well, although it can also leave a residual wave bias if the coherence between the vertically separated points is poor. A third method of horizontal differencing with adaptive filtering (Horizontal AF), which was predicted to perform well for sinusoidal, monochromatic waves, was found to perform poorly for conditions in

the coastal ocean, leaving a very large residual wave bias.

Error remaining in beam velocities after one of the differencing methods is applied can be attributed to residual wave bias, turbulence correlation between the two points chosen for differencing, or correlation between the waves and the turbulence. The turbulence correlation error, which arises if the chosen bin separation is too small, causes underestimation of the beam velocity variances. A marked trend of increasing residual wave error in beam velocity variance with increasing bin separation was observed for the Variance Fit method, due to increasing phase difference between the beam velocities at the chosen bins. However, the difference between opposing beam velocity variances, from which the Reynolds stress is derived, was unaffected by bin separation because both opposing beams were affected by a similar wave bias. Beam velocity variances computed using the Vertical AF method were relatively insensitive to bin separation above the lower limit determined by turbulence scales, suggesting that the Vertical AF method does not leave a consistent residual wave bias that is dependent on bin separation.

Reynolds stresses computed using both the Variance Fit and Vertical AF methods seem physically reasonable and yield bottom drag coefficients consistent with those reported in the literature. However, both methods become less accurate with increasing wave velocity, suggesting that both methods leave residual wave error. The Variance Fit method contains inherent wave error while the Vertical AF method leaves residual wave error if an adequate linear transfer function relating the wave velocities at the selected bins cannot be found. The performance of the Vertical AF method is expected to improve as faster ping rates become possible and as single ping velocity measurements become more accurate. Additionally, hybrid methods utilizing information from all four beams as well as pressure measurements offer further potential for improving ADCP turbulence measurements in wavy environments.

Acknowledgments. We thank Neil Davies, Frank Murphy, Nick Nidzieko, and Alyson Santoro for help with logistics and field work in Moorea. We would like to acknowledge Brian Gaylord, Cameron McDonald, Mike Moss, Brent Mardian, J. M. Ecker, Clint Nelson, Katie Arkema, Hannah Stewart, Dan Reed, and Sally MacIntyre for making the Santa Barbara deployment possible. Thanks also to the anonymous reviewer for his/her constructive suggestions. Funding was provided by the National Science Foundation (CTS-0335346, OCE99-82105, OCE-0417412, OCE-0622967) and by the University of California Marine Council Coastal Environmental Quality Initiative (04-T-CEQI-08-0048).

APPENDIX

Formulation of Vertical AF Method

The Variance Fit method is formulated as a differenced quantity squared; that is,

$$\widehat{\overline{u'^{(1-2)^2}_{\text{beam}}}} = \overline{\Delta u^{(1)^2}_{\text{beam}}}. \tag{A1}$$

This formulation can be interpreted as an estimate of the variance somewhere between the measurement locations $z^{(1)}$ and $z^{(2)}$. The residual wave error is $\epsilon_{\text{wave}} = \overline{(\Delta\tilde{u}^{(1)}_{\text{beam}})^2}$.

For ease of interpretation, the Vertical AF method was formulated in this paper as a differenced quantity multiplied by a nondifferenced quantity; that is,

$$\widehat{\overline{u'^{(1)^2}_{\text{beam}}}} = \overline{\Delta u^{(1)}_{\text{beam}} u^{(1)}_{\text{beam}}}. \tag{A2}$$

This formulation can be interpreted as the estimate of the variance of the along-beam component of turbulent velocity fluctuations at one of the measurement locations $z^{(1)}$. The residual wave error in this case is $\epsilon_{\text{wave}} = \overline{\tilde{u}^{(1)}_{\text{beam}} \Delta\tilde{u}^{(1)}_{\text{beam}}}$.

At first glance, it may seem the first formulation [Eq. (A1)] leaves a smaller residual wave error, but it can be shown that, because of properties of the linear transform $\mathcal{L}$, the two formulations [Eqs. (A1) and (A2)] are identical for the Vertical AF method. Beginning with the right-hand side of Eq. (A2),

$$\overline{\Delta u^{(1)^2}_{\text{beam}}} = \overline{u^{(1)^2}_{\text{beam}}} + \overline{[\mathcal{L}(u^{(2)}_{\text{beam}})]^2} - \overline{2u^{(1)}_{\text{beam}} \mathcal{L}(u^{(2)}_{\text{beam}})}. \tag{A3}$$

From Eq. (20), the linear transform can be written $\mathcal{L}(u^{(2)}_{\text{beam}}) = \mathbf{A}\mathbf{s}$; hence $\overline{[\mathcal{L}(u^{(2)}_{\text{beam}})]^2} = (1/N)(\mathbf{A}\mathbf{s})^{\mathrm{T}}\mathbf{A}\mathbf{s}$ and $\overline{u^{(1)^{\mathrm{T}}}_{\text{beam}} \mathcal{L}(u^{(2)}_{\text{beam}})} = (1/N)\mathbf{u}^{(1)^{\mathrm{T}}}_{\text{beam}}\mathbf{A}\mathbf{s}$. Therefore,

$$\begin{aligned}
\overline{[\mathcal{L}(u^{(2)}_{\text{beam}})]^2} &= \frac{1}{N}(\mathbf{A}\mathbf{s})^{\mathrm{T}}(\mathbf{A}\mathbf{s}) \\
&= \frac{1}{N}[\mathbf{A}(\mathbf{A}^{\mathrm{T}}\mathbf{A})^{-1}\mathbf{A}^{\mathrm{T}}\mathbf{u}^{(1)}_{\text{beam}}]\mathbf{A}\mathbf{s} \\
&= \frac{1}{N}\mathbf{u}^{(1)^{\mathrm{T}}}_{\text{beam}}\mathbf{A}(\mathbf{A}^{\mathrm{T}}\mathbf{A})^{-1}\mathbf{A}^{\mathrm{T}}\mathbf{A}\mathbf{s} \\
&= \frac{1}{N}\mathbf{u}^{(1)^{\mathrm{T}}}_{\text{beam}}\mathbf{A}\mathbf{s} \\
&= \overline{u^{(1)}_{\text{beam}} \mathcal{L}(u^{(2)}_{\text{beam}})}.
\end{aligned} \tag{A4}$$

Hence,

$$\begin{aligned}\overline{\Delta u_{\text{beam}}^{(1)\,2}} &= \overline{u_{\text{beam}}^{(1)\,2}} + \overline{u_{\text{beam}}^{(1)}\mathcal{L}(u_{\text{beam}}^{(2)})} - 2\overline{u_{\text{beam}}^{(1)}\mathcal{L}(u_{\text{beam}}^{(2)})} \\ &= \overline{u_{\text{beam}}^{(1)\,2}} - \overline{u_{\text{beam}}^{(1)}\mathcal{L}(u_{\text{beam}}^{(2)})} \\ &= \overline{u_{\text{beam}}^{(1)}\Delta u_{\text{beam}}^{(1)}}. \end{aligned} \quad \text{(A5)}$$

Thus the two formulations are identical for the Vertical AF method.

REFERENCES

Agrawal, Y. C., and D. G. Aubrey, 1992: Velocity observations above a rippled bed using laser Doppler velocimetry. *J. Geophys. Res.,* **97,** 20 249–20 259.

Bendat, J. S., and A. G. Piersol, 2000: *Random Data: Analysis and Measurement Procedures.* 3rd ed. Wiley, 594 pp.

Benilov, A. Y., and B. N. Filyushkin, 1970: Application of methods of linear filtration to an analysis of fluctuations in the surface layer of the sea. *Izv. Acad. Sci. USSR Atmos. Oceanic Phys. Engl. Transl.,* **6,** 810–819.

Bromirski, P. D., D. R. Cayan, and R. E. Flick, 2005: Wave spectral energy variability in the northeast Pacific. *J. Geophys. Res.,* **110,** C03005, doi:10.1029/2004JC002398.

Dean, R. G., and R. A. Dalrymple, 1991: *Water Wave Mechanics for Engineers and Scientists.* World Scientific, 353 pp.

Dewey, R. K., and W. R. Crawford, 1988: Bottom stress estimates from vertical dissipation rate profiles on the continental shelf. *J. Phys. Oceanogr.,* **18,** 1167–1177.

Feddersen, F., and A. J. Williams III, 2007: Direct estimation of the Reynolds stress vertical structure in the nearshore. *J. Atmos. Oceanic Technol.,* **24,** 102–116.

Fugate, D. C., and R. J. Chant, 2005: Near-bottom shear stresses in a small, highly stratified estuary. *J. Geophys. Res.,* **110,** C03022, doi:10.1029/2004JC002563.

Gross, T. F., and A. R. M. Nowell, 1983: Mean flow and turbulence scaling in a tidal boundary layer. *Cont. Shelf Res.,* **2,** 1109–1126.

Herbers, T. H. C., and R. T. Guza, 1993: Comment on "Velocity observations above a rippled bed using laser Doppler velocimetry" by Y. C. Agrawal and D. G. Aubrey. *J. Geophys. Res.,* **98** (C11), 20 331–20 334.

Howarth, M. J., and A. J. Souza, 2005: Reynolds stress observations in continental shelf seas. *Deep-Sea Res. II,* **52,** 1075–1086.

Lohrmann, A., B. Hackett, and L. P. Røed, 1990: High resolution measurements of turbulence, velocity, and stress using a pulse-to-pulse coherent sonar. *J. Atmos. Oceanic Technol.,* **7,** 19–37.

Lu, Y., and R. G. Lueck, 1999: Using a broadband ADCP in a tidal channel. Part II: Turbulence. *J. Atmos. Oceanic Technol.,* **16,** 1568–1579.

Nidzieko, N. J., D. A. Fong, and J. L. Hench, 2006: Comparison of Reynolds stress estimates derived from standard and fast-ping ADCPs. *J. Atmos. Oceanic Technol.,* **23,** 854–861.

RD Instruments, 2005: Workhorse acoustic Doppler current profiler technical manual. RD Instruments P/N957-6150-00, 196 pp.

Reidenbach, M. A., S. G. Monismith, J. R. Koseff, G. Yahel, and A. Genin, 2006: Boundary layer turbulence and flow structure over a fringing coral reef. *Limnol. Oceanogr.,* **51,** 1956–1968.

Rippeth, T. P., E. Williams, and J. H. Simpson, 2002: Reynolds stress and turbulent energy production in a tidal channel. *J. Phys. Oceanogr.,* **32,** 1242–1251.

——, J. H. Simpson, E. Williams, and M. E. Inall, 2003: Measurement of the rates of production and dissipation of turbulent kinetic energy in an energetic tidal flow: Red Wharf Bay revisited. *J. Phys. Oceanogr.,* **33,** 1889–1901.

Shaw, W. J., and J. H. Trowbridge, 2001: The direct estimation of near-bottom turbulent fluxes in the presence of energetic wave motions. *J. Atmos. Oceanic Technol.,* **18,** 1540–1557.

Souza, A. J., and M. J. Howarth, 2005: Estimates of Reynolds stress in a highly energetic shelf sea. *Ocean Dyn.,* **55,** 490–498.

Stacey, M. T., S. G. Monismith, and J. R. Burau, 1999a: Observations of turbulence in a partially stratified estuary. *J. Phys. Oceanogr.,* **29,** 1950–1970.

——, ——, and ——, 1999b: Measurements of Reynolds stress profiles in unstratified tidal flow. *J. Geophys. Res.,* **104** (C5), 10 933–10 949.

Trowbridge, J. H., 1998: On a technique for measurement of turbulent shear stress in the presence of surface waves. *J. Atmos. Oceanic Technol.,* **15,** 290–298.

Whipple, A. C., R. A. Luettich, and H. E. Seim, 2006: Measurements of Reynolds stress in a wind-driven lagoonal estuary. *Ocean Dyn.,* **56,** 169–185.

Williams, E., and J. H. Simpson, 2004: Uncertainties in estimates of Reynolds stress and TKE production rate using the ADCP variance method. *J. Atmos. Oceanic Technol.,* **21,** 347–357.